Human Amyloid-β_{40} Kinetics after Intravenous and Intracerebroventricular Injections and Calcitriol Treatment in Rats In Vivo [S]

H. Benson Peng, Keumhan Noh, Sophie R. Pan, Victor Saldivia, Sylvia Serson, Anja Toscan, Inés A.M. de Lannoy,[1] and K. Sandy Pang[1]

Department of Pharmaceutical Sciences, Leslie Dan Faculty of Pharmacy, University of Toronto, Toronto, Ontario, Canada (H.B.P., K.N., K.S.P.) and InterVivo Solutions Inc., Mississauga, Ontario, Canada (S.R.P., V.S., S.S., A.T., I.A.M.d.L.)

ABSTRACT

Amyloid-β peptides of 40 and 42 amino acid lengths, which are synthesized in neurons and degraded in the brain and liver, have the potential to aggregate and form neuritic plaques in Alzheimer disease. The kinetics of human amyloid-β (hAβ) 40 were examined in the rat pursuant to intravenous and intracerebroventricular administration after pretreatment with calcitriol, the active vitamin D receptor ligand (6.4 nmol·kg^{-1} in 0.3 ml corn oil every other day for four intraperitoneal doses) to induce P-glycoprotein (P-gp) and enhance hAβ_{40} brain efflux. The interference of hAβ_{40} by media matrix that suppressed absorbance readings in the ELISA assay was circumvented with use of different calibration curves prepared in Standard Dilution Buffer, undiluted, 10–10,000 or 5-fold diluted plasma, or artificial cerebrospinal fluid. Simultaneous fitting of hAβ_{40} plasma and cerebrospinal fluid (CSF) data after intravenous and intracerebroventricular administration were described by catenary-mammillary models comprising of a central and two peripheral compartments, the brain, and one to four CSF compartments. The model with only one CSF compartment (model I) best fitted the intravenous data that showed a faster plasma decay $t_{1/2}$ and slower equilibration between plasma and brain/CSF. Calcitriol induction increased the brain efflux rate constant, k_{41} (1.8-fold), at the blood-brain barrier when compared with the control group, as confirmed by the 2-fold ($P < 0.05$) increase in brain P-gp relative protein expression.

SIGNIFICANCE STATEMENT

An accurate description of the kinetic behavior of human amyloid-β (hAβ) 40 is needed in defining the toxic peptide as a biomarker of Alzheimer disease. Modeling of hAβ_{40} data after intravenous and intracerebroventricular administration to the rat revealed an initially faster plasma half-life that reflected faster peripheral distribution but slower equilibration between plasma and brain/cerebrospinal fluid even with calcitriol pretreatment that increased P-glycoprotein protein expression and enhanced efflux clearance from brain.

Introduction

Amyloid-β (Aβ) of 40 and 42 amino acid lengths is formed via sequential cleavage of the amyloid precursor protein by β- and γ-secretases in neurons (Haass et al., 1992; Hartmann et al., 1997; Weidemann et al., 1999). These pathogenic peptides are precursors of plaque formation in Alzheimer disease (AD) (Hardy and Higgins, 1992) and contribute to the amyloid cascade hypothesis that centers on the concept that Aβ toxicity in brain is pivotal to AD pathology (Zlokovic et al., 2000). In humans, the fractional synthesis and clearance of Aβ

are 7.6% and 8.3% per hour, respectively (Bateman et al., 2006). The average Aβ production rate (6.6%–6.8% per hour) by β-secretase is similar between normal and AD subjects, whereas brain Aβ clearance is much lower for those diagnosed with AD ($\sim$5.2% per hour) compared with normal subjects (7.0%–7.6% per hour) (Mawuenyega et al., 2010). Aβ clearance across the blood-brain barrier (BBB) is 6-fold higher than the interstitial fluid bulk flow (Bell et al., 2007) and 2-fold higher than metabolism by neprilysin, the proteolytic enzyme in the microglia that degrades Aβ_{40} (Iwata et al., 2000; Qosa et al., 2014). Aβ_{40} clearance appeared to be injection site–specific since ^{125}I-Aβ_{40} and ^{14}C-sucrose injected into the lateral ventricles of rat brains were found to be rapidly distributed throughout the cerebrospinal fluid (CSF) and cleared into blood, whereas diffusion into brain tissue (parenchyma) was poor and negligible (Ghersi-Egea et al., 1996a,b). About 62% of ^{125}I-Aβ_{40} injected intracerebrally to the mouse brain is found effluxed across the BBB, whereas the remaining 38% was associated with degradation and CSF bulk flow (Qosa et al., 2014). These processes appear to be Aβ_{40}- or Aβ_{42}-dependent, since radiolabeled Aβ_{40} injected into the hippocampus

---

ABBREVIATIONS: Aβ, amyloid β; aCSF, artificial CSF; AD, Alzheimer disease; AIC, Akaike Information Criterion; AUC, area under the concentration-time curve; BAB, blood-arachnoid barrier; BBB, blood-brain barrier; BCSFB, blood-CSF barrier; CL, clearance; CM, cisterna magna; CSF, cerebrospinal fluid; Gapdh, glyceraldehyde-3-phosphate dehydrogenase; hAβ, human Aβ; HFIP, 1,1,1,3,3,3-hexafluoro-2-propanol; Lrp1, low-density lipoprotein receptor-related protein 1; LV, lateral ventricle; Mrp1, multidrug resistance-associated protein 1; P-gp, P-glycoprotein; SAS, subarachnoid space; SDB, Standard Dilution Buffer; TBS-T, Tris-buffered saline/Tween 20; WSSR, weighted sum of squared residuals.

is readily transported across the BBB (Iwata et al., 2000) to reach the liver for elimination (Ghiso et al., 2004; Tamaki et al., 2006), whereas radiolabeled Aβ42 injected into the hippocampus lingered and was mostly recovered in the brain (Iwata et al., 2005).

The efflux of Aβ peptides from the brain via the BBB and blood-cerebrospinal fluid barrier (BCSFB) to the peripheral circulation allows the peptides to reach peripheral degradation organs, namely the liver (Ghiso et al., 2004; Tamaki et al., 2006) and potentially the kidney (Yasojima et al., 2001). Currently, there is strong evidence that the liver is a major organ that contributes to Aβ peptide degradation (Marques et al., 2009; Maarouf et al., 2018). An imbalance of Aβ peptide accumulation and degradation in brain or liver or efflux from the brain across the BBB and BCSFB could contribute to the seeding effect, allowing for accumulation, aggregation, and insoluble senile plaque formation (Shibata et al., 2000; Zlokovic et al., 2000; Bates et al., 2009; Deane et al., 2009).

Currently, there has not been any cohesive description of human amyloid-β (hAβ) 40 kinetics. Aβ pharmacokinetic studies are scarce, and the results have been spurious. Different half-lives ($t_{1/2}$) of 2.5–3 minutes (Ghiso et al., 2004), 0.7–1.7 hours (Abramowski et al., 2008), and 2 hours (Cirrito et al., 2003) and some ranging from 26 to 240 minutes (Shibata et al., 2000) have been reported in mice in vivo. The disparity in the $t_{1/2}$ is likely due to inappropriate methodology (inadequate sampling or use of total radioactivity to represent Aβ), misinterpretation, aggregation problems of Aβ (Teplow, 2006), and/or interference in the ELISA (Lanz and Schachter, 2006). Whether CSF concentration is a good surrogate of the unbound brain concentration (Tang et al., 2009) and whether hAβ40 or the ratio of hAβ42/hAβ40 in plasma or CSF relate to the extent of cerebral amyloidosis or AD progression (Seppälä et al., 2010; Vergallo et al., 2019) are unknown. We initiated a study in rats with intravenous or intracerebroventricular administration of hAβ40 to appraise the complex kinetics of hAβ40 after calcitriol treatment. The rat, a larger rodent that does not synthesize hAβ40, was chosen for study since its size allows for sequential plasma and CSF sampling, and any variation in hAβ40 synthesis is nonexistent. A sound strategy that accounted for matrix interference by albumin, transthyretin, or α-2-macroglobulin, which quench the Aβ signal (Biere et al., 1996; Kuo et al., 1999; Lanz and Schachter, 2006; Alemi et al., 2016), in the sample was used to assay for hAβ40 in plasma and CSF. The pharmacokinetics of hAβ40, a substrate of P-gp (Lam et al., 2001), was studied after pretreatment with calcitriol, the active ligand of the vitamin D receptor (VDR) known to induce for P-gp in humans, mice, and rats (Durk et al., 2012, 2014).

Materials and Methods

Reagents and Chemicals. All reagents, chemicals, and calcitriol in powder form were obtained from Sigma-Aldrich (Mississauga, ON). Powdered hAβ40 peptide was purchased from Biopeptide Co., Inc. (San Diego, CA). The ELISA kit for the hAβ40 (KHB3841) assay and the primary mouse anti-rat P-gp antibody (C219) were purchased from ThermoFisher Scientific (Mississauga, ON), whereas the rabbit anti-rat neprilysin antibody (AB5458) was from Millipore Sigma (Etobicoke, ON), and rabbit anti–low-density lipoprotein receptor-related protein 1 (Lrp1) antibody (ab92544) and mouse anti-rat Gapdh (ab8245) antibodies were from Abcam (Cambridge, MA). The rat anti-Mp1 antibody (MC-106) was from Kamiya Biomedical (Seattle, WA). The goat anti-mouse or goat anti-rabbit IgG secondary antibody conjugated to horseradish peroxidase was procured from BioRad (Mississauga, ON). Artificial CSF (aCSF) was obtained from Harvard Apparatus (St. Laurent, QC).

Preparation of hAβ40 Stock Solution for Dosing. The hAβ40 peptide for dosing was prepared according to previously described reports (Stine et al., 2003; Teplow, 2006; Roychaudhuri et al., 2015). Briefly, the hAβ40 in powder form was solvated in 100% 1,1,1,3,3,3-hexafluoro-2-propanol (HFIP), made up to 1 mM (Stine et al., 2003) in the original glass vial, and left at room temperature until

a clear solution was obtained. The content was transferred to a 1.5-ml polypropylene microcentrifuge tube for evaporation of HFIP overnight in the fume hood. The clear peptide film was dried under vacuum in a SpeedVac rotary evaporator for 2 hours to ensure complete HFIP removal, and the resulting desiccated peptide film was redissolved in 10% (v/v) 0.06 N NaOH, 45% (v/v) double distilled H_2O, and 45% (v/v) PBS (20 mM sodium phosphate, pH = 7.4) to a 1–mg·ml^{-1} stock solution. This reconstituted hAβ40 peptide stock solution was sonicated over an ice bath (Branson) for 1 minute and then aliquoted and stored immediately at −80°C for future use. The preparation and storage of hAβ40 in this fashion ensured that the peptide was stable and reproducible for intravenous and intracerebroventricular administration. The integrity and stability of the 1 mg·ml^{-1} hAβ40 stock solution stored at −80°C up to a month was ascertained on different occasions with ELISA assay and a liquid chromatography tandem mass spectrometry procedure developed at InterVivo Solutions. Briefly, an AB Sciex 6500QTrap mass spectrometer with Exion LC system and autosampler, a Thermo ProSwift RP-4H column, and gradient elution (mobile phase A: 0.3% NH₄OH in water, mobile phase B: acetonitrile at 0.4 ml/min) were used over a run time of 4.7 minutes. The mass spectrometer was operated with a TIS interface and multiple-reaction monitoring in positive ion mode. Ion transitions that were used for quantitation were: hAβ40 m/z 1083.3 (M+4H]$^{4+}$) → 1054.2 with ^{15}N-Aβ40 (m/z 1096.3 (M+4H]$^{4+}$) →1066.9) as internal standard. hAβ40 was shown to be stable with one to four freeze-thaws. For intravenous dosing, the 1–mg·ml^{-1} stock solution was further diluted with PBS (1:4, v/v, pH 7.4, from GIBCO, catalog number 10010023; obtained from ThermoFisher Scientific) on the day of the experiment, whereas for intracerebroventricular dosing, the desiccated peptide film was used to prepare a 2 mg·ml^{-1} solution for administration. The concentrations of the intravenous and intracerebroventricular doses were first estimated by UV spectrophotometry (UV-1700; Shimadzu Scientific Instruments, Columbia, MD) at the wavelength of 280 nm because of the single Tyr residue present on the hAβ40 peptide (Jan et al., 2010), and concentration of the dosing solution was subsequently confirmed by ELISA.

ELISA. The primary 160 ng standard stock of hAβ40, which was provided by the manufacturer, was first dissolved with 1.6 ml of the Standard Reconstitution Buffer (55 mM sodium bicarbonate, pH 9) to obtain a 100 ng·ml^{-1} stock solution. This stock solution was diluted to 10,000 pg·ml^{-1} with the Standard Dilution Buffer (SDB) to prepare the eight standards by serial dilution (500 ro 7.81 pg·ml^{-1}) according to the protocol suggested by the manufacturer. The absorbances of the standards were measured at 450 nm (SpectraMax 340PC; Molecular Devices, Sunnyvale, CA) for construction of the calibration curve for the determination of plasma or CSF concentrations.

The presence of albumin, transthyretin, or α-2–macroglobulin could quench the Aβ signal and interfere with the ELISA assay for hAβ40 in plasma and CSF (Biere et al., 1996; Kuo et al., 1999; Lanz and Schachter, 2006; Alemi et al., 2016). The interference from plasma was examined by varying the proportion of rat plasma (from 0% to 95% plasma) in the hAβ40 standards, thus prepared as 1000, 2000, 5000, and 8000 pg·ml^{-1} (n = 3 in each set). Also, different media were used to prepare the standards of various calibration curves. The CSF standards were prepared in SDB (0, 10–10,000-fold, v/v) or aCSF or directly loaded as 50-μl aliquots onto the ELISA plate. The interference from rat plasma or aCSF was examined among calibration curves generated from undiluted blank plasma (50 μl direct loading), from 5- and 10–10,000-fold diluted plasma in SDB, or in 100% aCSF versus the calibration curve based on hAβ40 standards prepared in SDB.

In Vivo Experiments. All animal protocols were approved by the InterVivo Solutions Animal Care Committee, and studies were carried out in accordance with the principles of the Canadian Council on Animal Care. Male Sprague-Dawley rats, purchased from Charles River Laboratories (St. Constant, QC), were acclimated under a 12-hour light/dark cycle and given water and chow ad libitum at InterVivo Solutions for at least 5 days prior to dosing. The rats (318 ± 41.6 g) were weighed on the day of dosing.

The effect of corn oil, the vehicle for intraperitoneal injection of calcitriol, on hAβ40 kinetics was first investigated in absence of calcitriol. The hAβ40 dose was determined after a broad and exhaustive literature search on Aβ injections via intravenous, intracerebral or intracerebroventricular routes to various animal (guinea pigs, mice, and rats) models. In the first set of animals, the hAβ40 dose (68.5 ± 12.0 μg·kg^{-1}; n = 4) was administered intravenously to rats that were pretreated blank corn oil (0.3 ml) given every other day intraperitoneally for four doses for comparison with hAβ40 kinetics (64.5 ± 13.2 μg·kg^{-1} in saline, n = 12)

among control rats that were not pretreated with corn oil. In the second set of rats, $hA\beta_{40}$ kinetics after a single $hA\beta_{40}$ intracerebroventricular dose (48.0 ± 14.9 $\mu g \cdot kg^{-1}$ in corn oil, n = 4) were compared with those after intravenous dosing (data from first set were combined to give n = 16, since corn oil did not affect $hA\beta_{40}$ kinetics). For the last set, rats were pretreated with calcitriol (6.4 $nmol \cdot kg^{-1}$ in 0.3 ml corn oil every other day for four doses, intraperitoneally) and then administered a single intravenous (73.5 ± 6.02 $\mu g \cdot kg^{-1}$; n = 7) or intracerebroventricular (20.3 ± 1.30 μg kg^{-1}; n = 5) dose of $hA\beta_{40}$ 1 day after completion of the calcitriol pretreatment regimen.

Surgery was performed under 4% isoflurane in oxygen for anesthesia and 1–3% for maintenance, and rats were allowed to fully recover for 1 day before dosing. Catheters were implanted into the jugular vein for intravenous dosing or the lateral ventricle (LV) for intracerebroventricular dosing, into the carotid artery for serial blood sampling, and into the cisterna magna (CM) for CSF collection. The common bile duct was cannulated for the collection of bile in three rats (intravenous control group) that remained anesthetized during dosing and sampling. For intravenous dosing, the jugular vein catheter (CX-2011S; BASi, West Lafayette, IN) was prefilled with heparinized (40 U/ml) physiologic saline solution to prevent blood coagulation. An $hA\beta_{40}$ (~0.2 ml) bolus dose was injected into the jugular vein followed by flushing with ~0.1 ml of heparinized saline. For intracerebroventricular dosing, an intracerebroventricular guide cannula (P1 technologies, Roanoke, VA) was placed into the right lateral ventricle of the brain (stereotactic coordinates: −0.92 Anteroposterior or AP, −1.3 Lateral or L, and −3.1 Dorsoventral or DV relative to the bregma) with facilitation of a stereotaxic instrument. The dosing solution (0.01 ml) was administered via a 1-ml Hamilton glass microsyringe (inner diameter 1.46 mm) fitted to the intracerebroventricular injection catheter at 1 $\mu l \cdot s^{-1}$ using a Harvard Apparatus Pump 11 elite system. Serial blood sampling (0.15 ml) was performed after both intravenous and intracerebroventricular injections via the carotid artery catheter at times 0, 0.5, 1, 2, 5, 10, 15, 30, 45, 60, 90, 120, 150, and 180 minutes postdose, and sampled volumes were replaced with heparinized saline. Plasma was obtained by immediate centrifugation of blood at 4000g for 10 minutes at 4°C. For CSF sampling, a BSIL-T015 0.015ID tubing cannula (Plymouth Meeting, PA) was inserted into the cisterna magna (CM) and kept in place by a metal pin stopper (SP22/12). Serial CSF sampling (10–50 μl) was conducted via the cisterna magna cannula at times 0, 15, 30, 60, 120, and 180 minutes. A BASi CX-8000S catheter was inserted into the common bile duct for sampling (untreated intravenously injected saline-treated rats, n = 3) at 30-minute intervals. Urine was collected into pretared tubes throughout the 180 minutes of experimentation. After the last sample collection, rats were sacrificed by exsanguination under isoflurane anesthesia and transcardially perfused with 50 ml ice-cold physiologic saline solution prior to tissue collection. Hemibrains, liver (minced), kidney, and all subsequent samples were flash-frozen with liquid nitrogen, weighed, and stored at −80°C for future analysis.

Noncompartmental Analysis. All plasma concentrations and amounts in bile or urine were normalized to the dose and expressed as $\%dose \cdot ml^{-1}$ (frequency) and % dose, respectively. The dose normalization facilitated data comparison among studies even when the doses differed slightly. Noncompartmental analysis was conducted for plasma and CSF $hA\beta_{40}$ data. The area under the concentration-time curve (AUC) to time infinity, AUC_∞, was obtained by summing the area up to last sampling point based on the trapezoidal rule ($AUC_{0\text{-last}}$), and the extrapolated area under the curve was obtained upon dividing the concentration of the last sample, C_{last}, by the terminal decay constant. Total body (plasma) clearance (CL_{plasma}) and CSF clearance (CL_{CSF}) after intravenous (IV) and intracerebroventricular (ICV) injections, respectively, were calculated as $dose_{IV}/AUC_{\infty,plasma}$ and $dose_{ICV}/AUC_{\infty,CSF}$; biliary clearance was determined as $f_{bile} \cdot CL_{plasma}$, in which f_{bile} = $hA\beta_{40}$ amount in bile/$dose_{IV}$.

Compartmental Modeling. Compartmental models (Fig. 1) were constructed for data fitting after intravenous and intracerebroventricular administration of $hA\beta_{40}$ with ADAPT5. We employed models that embellish physiologic meanings. After extensive preliminary modeling, a three-compartment model (one central and two peripheral compartments) was considered as more consistent with data than the one- or two-compartment model. Fits to one- or two-compartment models did not predict the data well (unpublished data). To the central compartment, a brain and additional (1, 2, or 4) CSF compartments were included (Fig. 1). Model I (Fig. 1A) is the simplest model whereby the entire volume of CSF is present in the ventricles/choroid plexus/CM and subarachnoid space (SAS). Model II distinguishes the site of intracerebroventricular injection (LV)

from the site of CSF sampling downstream. In model III, the four CSF compartments correspond to the four ventricles, CM (sampling compartment), and SAS, as modeled by Westerhout et al. (2012) and de Lange et al. (2017). The number of CSF compartments is based on the flow of CSF, being formed from the four ventricles at the choroid plexus then flowing from the first two LVs through the single midline third ventricle and midline fourth ventricle to the CM and then upward over the convexities of the brain in the SAS, where CSF is absorbed through the arachnoid villi at the top of the brain into the superior sagittal sinus of the venous circulation (Pardridge, 2016). From the CM, CSF flows downward to the spinal cord (Fig. 1C) (Yamamoto et al., 2018).

In models I, II, and III, the intercompartmental transfer or distributional rate constants between the central, peripherals, brain, and CSF compartments are denoted as k_{12}, k_{21} $k_{13}, k_{31}, k_{14}, k_{41}, k_{45}, k_{15}, k_{51},$ and k_{54}. V_1, V_2, V_3, and V_4 are the volumes of distribution for the central, two peripheral, and brain compartments, respectively, and the volumes V_5, V_6, V_7 and V_8 are for the CSF compartments. V_4 was taken as 1.8 g (Davies and Morris, 1993). In all the models, the elimination rate constants k_{10}, k_{40}, and k_{50} denote the possible degradation pathways of $hA\beta_{40}$ from the central, brain, and CSF compartments, respectively: degradation by neprilysin in brain is denoted by k_{40}, whereas degradation in CSF occurs via the insulin-degrading enzyme (k_{50}), which is normally considered to be an insignificant pathway (Saido and Leissring, 2012). There are at least four barriers: the BBB exists between the brain capillary endothelial cells containing tight junctions and brain parenchyma, where P-gp is present apically (k_{41}); there is a barrier from the ventricular ependymal cells that presents as a relatively leaky barrier between the CSF and brain interstitial fluid, with k_{45} for efflux and k_{54} for the return from CSF to brain (Takasawa et al., 1997); the BAB lies between the fenestrated blood vessels in the meninges and the CSF in the arachnoid space formed by tight junctions of the arachnoid epithelial cells (Yasuda et al., 2013), where return of CSF to the circulation also occurs; and lastly, there is the BCSFB formed by tight junctions between the choroid plexus epithelial cells, which restrict the movement of molecules that leak from the fenestrated capillaries into the extracellular compartment of the choroid plexus then into the CSF (k_{15} for influx from blood at the ventricular choroid plexus, and k_{51} for return to peripheral blood). For model I, in which there is only one CSF compartment, k_{51} now represents the sum total of the return from BCSFB, BAB, and CSF bulk flow. For model II, k_{51} represents the return from the BCSFB, and k_{61} represents the return CSF flow and efflux functionality at the arachnoid villi (BAB). For model III, k_{51} represents the return from the BCSFB with k_{81} representing the return CSF flow and efflux functionality at the BAB.

Fitting. The ADAPT5 System Analysis Software (Biomedical Simulations Resource, Version 5.0.53; University of Southern California, Los Angeles, CA) was used for data fitting with the Maximum-Likelihood Expectation Maximization algorithm. Initial estimates were determined from curve-stripping analysis. Simultaneously fitting of both the control and calcitriol data sets was not successful. First, only first-order conditions are assumed to prevail. The first fit was based on the combined control data of $hA\beta_{40}$ in plasma and CSF after intravenous and intracerebroventricular injections into the rat. The second fit was performed on model fitting to the combined data from intravenous and intracerebroventricular injections to the treated rats. Preliminary fitting showed that inclusion of the rate constant k_{15} in model I did not affect the fit because the value was very low and could be omitted. The same was observed for k_{51}. For subsequent fits to models II and III, setting k_{15} or $k_{51} = 0$ did not affect the fit (Supplemental Tables 1 and 2), suggesting that the net transport at the BCSFB is insignificant. The decision agrees with reports on the low permeability of unconjugated human Aβ in the rat (Saito et al., 1995; Poduslo et al., 1999; Kandimalla et al., 2005) and that the activity at the BCSFB is much lower (1/30) than that at the BBB (Morris et al., 2017).

As a starting point, model I (Fig. 1A) was used to fit the $hA\beta_{40}$ intravenous and intracerebroventricular data sets in absence of calcitriol treatment. The resulting fit provided both individual and population best fits for the control (non-calcitriol treated) data to render final estimates. These rate constants were then used as initial estimates to fit the intravenous and intracerebroventricular calcitriol treatment data in the second and third fits. Since preliminary modeling showed that volume of the CSF compartment ($V_{5,CSF}$) was increased 5-fold after calcitriol treatment without any compelling physiologic reasons, the volume estimates of $V_{1,plasma}$ and $V_{5,CSF}$ from the first fit (control data set) were fixed for the second and third fits (calcitriol treatment data, labeled as "A" for model 1A and "B" for model 1B) (see Table 1). Similar strategies were used for models II and III by
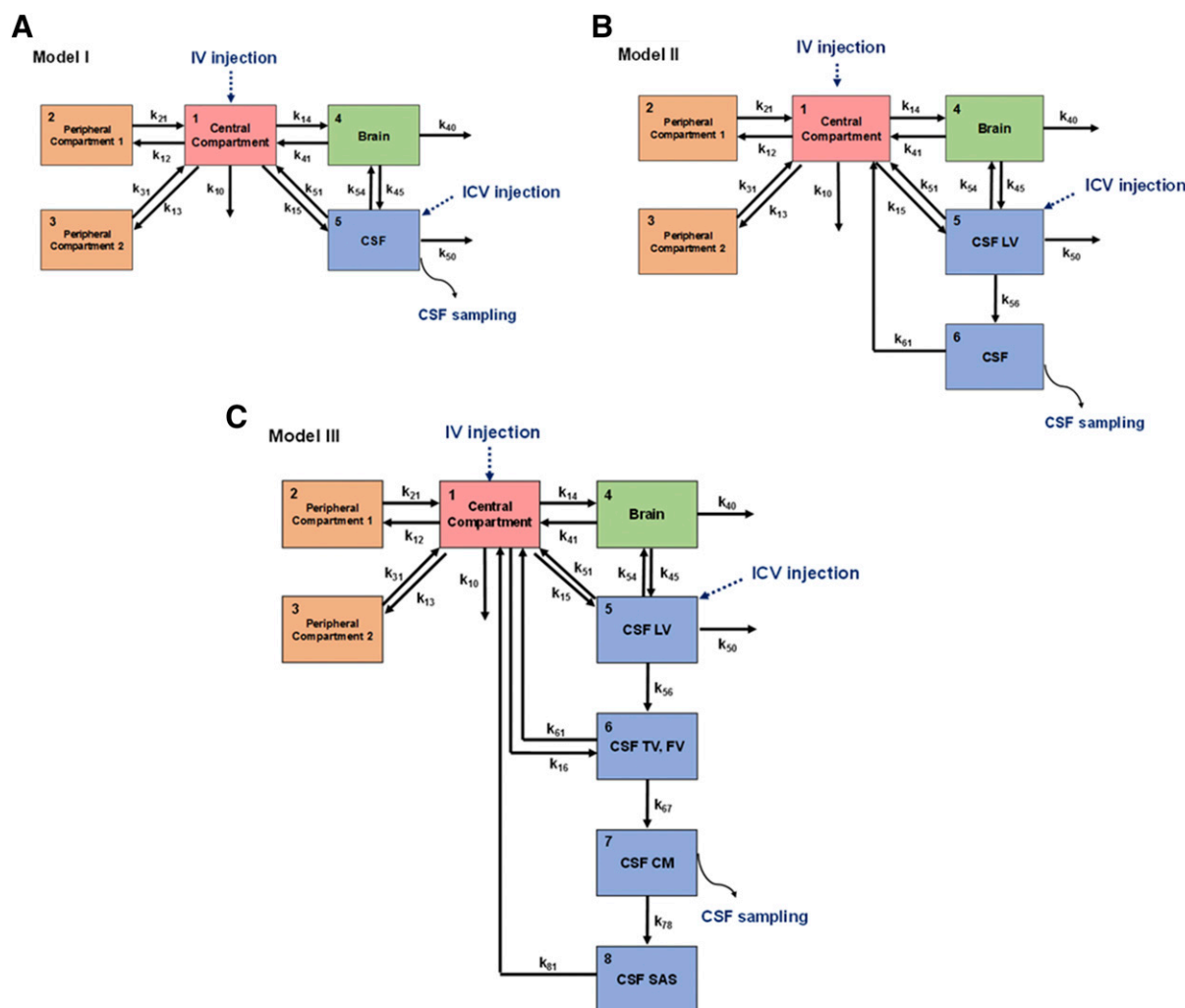
Fig. 1. Models I, II, and III are depicted in (A), (B), and (C), respectively, for the fitting of the plasma and CSF data after intravenous (IV) and intracerebroventricular (ICV) hAβ$_{40}$ administration. FV, fourth ventricle; TV, third ventricle.

fixing the CSF return rate constant, k$_{51}$, k$_{61}$, or k$_{81}$ (see Supplemental Tables 2 and 3). We also assigned physiologic volumes for fitting (Davies and Morris, 1993) for model II. For best fits, graphs were visualized (prediction plots) as well as statistical outputs, the weighted sum of squared residuals (WSSR), and Akaike Information Criterion (AIC); the lowest number suggests the best fit. We examined the *F*-test statistic (with use of degrees of freedom and WSSR to calculate the *F*-score for comparison with the critical *F*-value, with the significance level, α, as 0.05) for the best fit (Boxenbaum et al., 1974).

Western Immunoblotting. Rat hemibrains were homogenized in 5× homogenizing buffer containing protease inhibitors (1:100; v/v), and the brain homogenate was subsequently centrifuged at 3000*g* for 10 minutes at 4°C (Chow et al., 2011). The resulting brain supernatant was further diluted with homogenizing buffer and centrifuged at 33,000*g* for 60 minutes at 4°C. The resultant pellet or non-nuclear crude membrane fraction was resuspended in 200–300 μl of resuspension buffer containing protease inhibitor (1:100; v/v) (Chow et al., 2011), and protein concentration was determined by the Lowry method (Lowry et al., 1951). Aliquots containing 40 μg of non-nuclear (crude) membrane protein in brain for P-gp, neprilysin, and multidrug resistance-associated protein 1 (Mrp1) and 5 μg for Lrp1 were resolved with 10% SDS–polyacrylamide gel electrophoresis. The resolved proteins were wet-transferred (BioRad) onto nitrocellulose membranes (GE Health, Mississauga, ON) and blocked with 5% skim milk dissolved in Tris-buffered saline + 0.1% Tween-20 (1X TBS-T) at room temperature for 1 hour. After this step, blots were washed once with TBS-T solution, cut, and probed overnight at 4°C with respective primary anti–P-gp (1:500; v/v), anti-neprilysin (1:1000; v/v), anti-Mrp1 (1:50; v/v), anti-Lrp1 (1:50,000; v/v), and anti-Gapdh (1:15,000; v/v) antibodies in 2% skim milk TBS-T

solution. The blots were washed three times with TBS-T (15 minutes for each wash) and incubated further at room temperature for 2 hours with goat anti-mouse or rabbit IgG secondary antibody conjugated to horseradish peroxidase (1:1000 for P-gp, neprilysin, Mrp1, Lrp1, and 1:10,000 for Gapdh; v/v) in 2% skim milk TBS-T solution. After 2 hours of incubation, blots were washed again three times with TBS-T (15 minutes for each wash) and imaged by the enhanced chemiluminescence reagent (GE Health, Amersham) with ChemiDoc MP (BioRad). The band intensities were quantified by densitometry and normalized to the housekeeping protein, Gapdh.

Statistical Analysis. All concentration data were normalized to dose and expressed as %dose·ml^{-1}, and data are expressed as mean ± S.D. The Student's unpaired *t* test was conducted for the comparison of Western immunoblots and parameters obtained for untreated and corn oil–treated rats by noncompartmental analysis, and the Wilcoxon rank sum test (nonparametric test, R) was conducted for individual parameters from population data set, and the significant *P* value was <0.05.

Results

Quantitation of hAβ$_{40}$

Calibration curves that were generated from different types of media (SDB, 10–10,000-fold diluted plasma, 5-fold diluted plasma by mixing 10 μl plasma with 40 μl SDB or 50 μl undiluted plasma, or aCSF) were used for appraisal of the matrix effect. The limit of quantitation was 7.81 pg·ml^{-1} for plasma and CSF hAβ$_{40}$ concentrations. Clearly, the
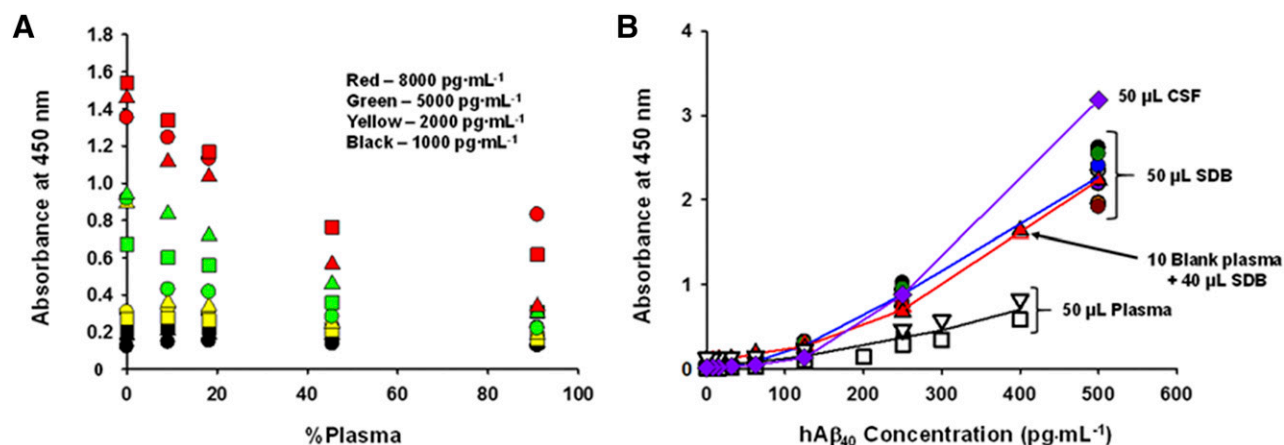
Fig. 2. Effect of plasma on suppressing absorbance signal (optical density or ODS) in the $hA\beta_{40}$ ELISA assay, postdilution (A), with ODS prepared with different calibration standards in four different matrices (B)—50 μl SDB, 10 μl plasma + 40 μl SDB, undiluted rat plasma, or aCSF—after sequential dilution with plasma or aCSF matrices to generate the calibration curves. The same colored symbol was used for standards prepared within the same calibration curve.

matrix effect that resulted in quenching of absorbance by plasma components was observed among the 1000–8000-pg·ml^{-1} samples (Fig. 2A); the greater the % rat plasma, the greater the magnitude of quenching. Signal suppression by the undiluted plasma was about 50% for the 8000–pg·ml^{-1} sample. The calibration curves prepared in SDB and 5-fold diluted plasma were essentially identical, whereas values of the standards generated in 50 μl undiluted plasma were lower (Fig. 2B). The calibration curves prepared in SDB and 5-fold diluted plasma were essentially identical, whereas values of standards generated in 50 μl undiluted plasma were diminished (Fig. 2B). For standards prepared in aCSF, the assayed value for the highest calibration standard was higher than that prepared in SDB or the 10- to 10,000-fold diluted plasma, but values for other calibration standards were all similar (Fig. 2B). Hence, multiple calibration curves were prepared in different matrices and different dilutions of the sample (Fig. 2B). Since most of the measured concentrations were between 7.81 and 250 pg·ml^{-1}, the resulting concentrations after interpolation were similar for the samples prepared in SDB or in plasma samples with sufficiently high dilution (>10–10,000-fold dilution with SDB). The calibration curve prepared in SDB was deemed appropriate for the determination of $hA\beta_{40}$ samples at earlier time points (>10–10,000-fold dilution), whereas for the late-in-time undiluted plasma samples (last data point at 180 minutes), the calibration curve that was prepared in undiluted rat plasma was used for quantitation.

Pharmacokinetics of $hA\beta_{40}$

Noncompartmental Modeling of Intravenous Data in Untreated versus Corn Oil–Treated Rats. We first tested whether corn oil, the vehicle for calcitriol administration, affected the kinetics of $hA\beta_{40}$ in groups of rats. In both groups of rats given intravenous $hA\beta_{40}$, similar multiexponential decay profiles were observed for the $hA\beta_{40}$ in plasma; CSF concentrations rose quickly and remained quite constant over the 180 minutes of sampling (Fig. 3A). The apparent terminal $t_{1/2}$ of $hA\beta_{40}$, estimated by regression of the log-linear portions of the plasma decay curves, were similar (24.5 ± 0.05 and 16.8 ± 5.66 minutes for the untreated and the corn oil–treated rats (Fig. 3B), respectively; $P > 0.05$), whereas those for CSF were considerably longer (75.5 ± 17.9 and 47.9 ± 20.9 minutes, respectively; $P > 0.05$). The $AUC_{\infty,plasma}$ (extrapolated to infinity) normalized to the dose for the injections in saline- and corn oil-(vehicle) pretreated rats were not different ($P > 0.05$; Table 1), yielding similar plasma clearances (CL_{plasma}) of 17.9 ± 6.20 and 23.2 ± 2.21 ml·min^{-1}·kg^{-1} for both groups. The total amounts recovered in

bile collected for untreated rats and the fraction of dose (f_{bile}) excreted into bile were both very low, and $hA\beta_{40}$ was undetectable in urine. The partition coefficient for CSF/plasma ($K_{p,CSF:plasma}$), calculated as ratio of $AUC_{\infty,CSF}/AUC_{\infty,plasma}$, was low and similar (0.0085 ± 0.00211 and 0.0099 ± 0.00680, $P > 0.05$) between the untreated and corn oil–treated rats. The composite data showed that corn oil did not interfere with the kinetics of $hA\beta_{40}$ (Table 1).

Compartmental Modeling and Fitting of Data after Intravenous and Intracerebroventricular Injections. Because the $hA\beta_{40}$ concentration-time profiles of the control rats, with or without corn oil treatment, were similar after intravenous $hA\beta_{40}$ dosing, data for this first group of rats were combined and consolidated as the control intravenous group (n = 16). These intravenous data that exhibited the shorter $t_{1/2}$ in plasma were for comparison with the control data after intracerebroventricular injections (n = 4), which showed that $hA\beta_{40}$ plasma and CSF concentrations decayed in unison. All models (Fig. 1) were used for fitting of the intravenous and intracerebroventricular data for the control groups (fit 1) and then for the intravenous and intracerebroventricular data for the treatment groups (fit 2). Preliminary fits showed minor and 5-fold changes in $V_{1,plasma}$ and $V_{5,CSF}$, respectively, for model I. Because there is no physiologic basis of these volume changes, we constrained these parameters and assigned the fitted estimates from the first fit as volumes of plasma and CSF for the second fit ("A" versions of models); another added constraint was carried out by setting the return CSF clearance: $k_{51} \cdot V_{5,CSF}$, $k_{61} \cdot V_{6,CSF}$, and $k_{81} \cdot V_{8,CSF}$ for models I, II, and III, respectively ("B" versions of the models). The F scores for all models were not significantly different from model I for all fits, although differences in WSSR and AIC were noted (Table 2). The key changes of the derived rate constants from models I, IA, and IB (Table 3), and models II, IIA, IIB, III, IIIA, and IIIB (Supplemental Figs. 1 and 2; Supplemental Tables 1 and 2) are summarized. Statistically, best fits were observed for model I and IA (Fig. 4), and $V_{5,CSF}$, whether being constraint or not, is not important. Then model II, which revealed low WSSR and AIC values (Table 2) and excellent prediction plots (Supplemental Fig. 1), was also found to be satisfactory, but model II fits were associated with higher CVs (Supplemental Table 1). Fits for models IB, IIA, and IIB; all model III (Fig. 4; Supplemental Figs. 1 and 2); and other models (unpublished data) were poorer. For the treatment data, the intracerebroventricular CSF data for models IIB and IIC were consistently overpredicted, whereas the intracerebroventricular plasma data for Models IB and III were consistently underpredicted (Fig. 4; Supplemental Figs. 1 and 2). Additionally, more complex models,
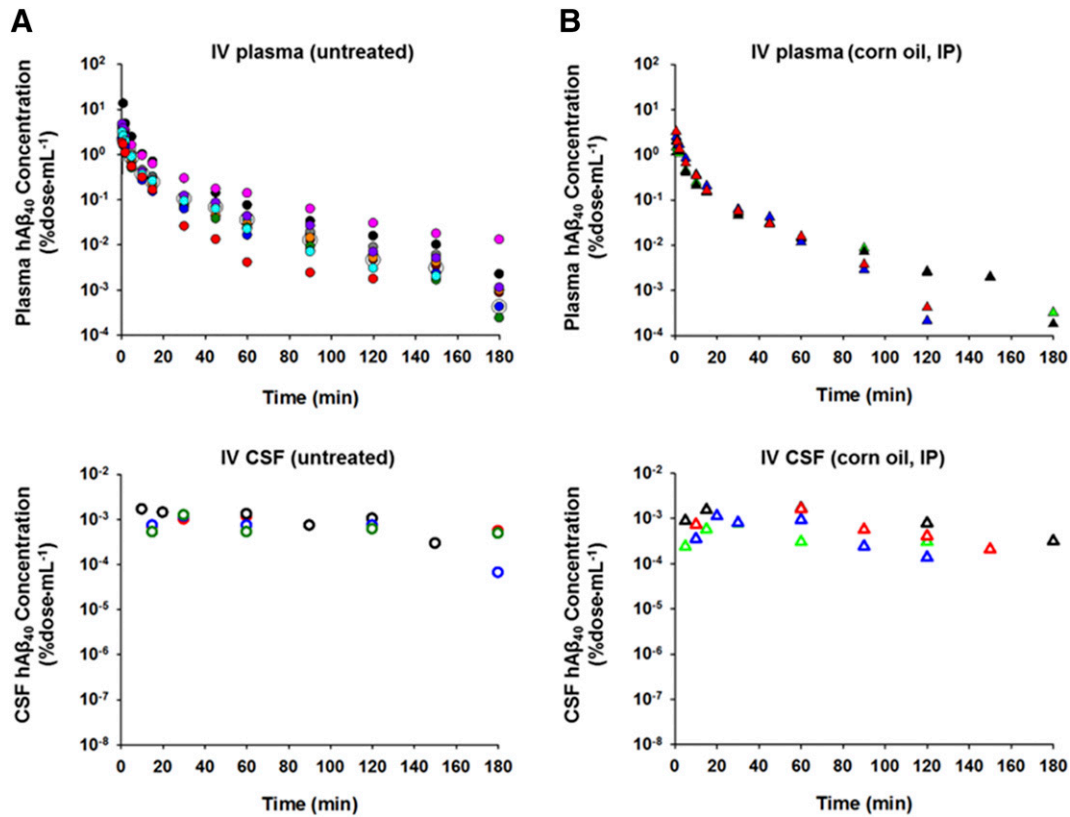
Fig. 3. Rat plasma and CSF concentration-time profiles (concentrations normalized to dose, %dose·ml^{-1}) after intravenous (IV) administration of hAβ40 to untreated (n = 12, left panels), A; and corn oil–treated (q2d ×4; right panels, n = 4) rats, B. Serial samples obtained from the same rat were denoted with the same symbol and color. IP, intraperitoneal.

including addition of an interstitial fluid or glymphatic compartment or a semi–physiologically based pharmacokinetic model, did not improve the fit to our data (unpublished data). The data for the nontreatment and treatment groups were within the predicted 5% and 95% confidence interval (shaded area between dotted red or blue lines) for model I (Fig. 5).

For model I, k_{41}, k_{45}, and k_{51} were increased 1.8-, 3.4-, and 5.4-fold, respectively; $V_{5,CSF}$ was increased 5.3-fold ($P < 0.05$) after calcitriol treatment. This volume change was found to be unimportant since model IA (assigning $V_{5,CSF}$ and $V_{1,plasma}$ as constants) also predicted the data well (Fig. 4). Upon restraining the volumes of plasma and CSF (model IA), k_{41}, k_{45}, and k_{51} were increased 1.7-, 1.6-, and 8.2-fold, respectively. The increase in k_{51} could be explained when P-gp, which is present abundantly at the arachnoid villi (BAB) (Yasuda et al., 2013), is also induced by calcitriol. Upon further restraining k_{51}, $V_{1,plasma}$, and $V_{5,CSF}$ as constants (model IB), k_{41} and k_{45} were increased 1.25- and 2.75-fold, respectively. In all fits, the CSF ($k_{50}·V_{5,CSF}$) and brain ($k_{40}·V_{4,brain}$) degradation clearances were unchanged with calcitriol treatment (Table 3). A closer look at the calcitriol-treated group revealed a slightly but insignificantly faster terminal phase when compared with the control group. The CL_{plasma} ($k_{10}·V_{1,plasma}$) was increased significantly only for model I from 21.8 to 25.8 ml min^{-1}kg^{-1} with calcitriol

TABLE 1

Noncompartmental parameters for hAβ40 after single intravenous injections to untreated and intraperitoneally corn oil–treated rats (absence of calcitriol treatment)[a]

Parameter	Without Calcitriol Treatment		P Value
	hAβ40 i.v. (n = 12)	hAβ40 i.v. and Corn Oil (i.p.) (n = 4)	
Rat weight (g)	282 ± 24.9	339 ± 76.2	NS[b]
Dose (μg·kg^{-1})	64.5 ± 13.2	68.5 ± 12.0	NS
AUC$_{0-\infty,plasma}$ (%dose·min·ml^{-1})[c]	24.2 ± 14.7	13.2 ± 2.56	NS
AUC$_{0-\infty,CSF}$ (%dose·min·ml^{-1})[c]	0.121 ± 0.040	0.124 ± 0.063	NS
Observed t$_{1/2,terminal\ plasma}$ (min)	24.5 ± 4.05	16.8 ± 5.66	NS
Observed t$_{1/2,terminal\ CSF}$ (min)	75.5 ± 17.9	47.9 ± 20.9	NS
CL$_{plasma}$ (ml·min^{-1}·kg^{-1})	17.9 ± 6.20	23.2 ± 2.21	NS
CL$_{bile}$ = f$_{bile}$·CL$_{plasma}$ (ml·min^{-1}·kg^{-1})	0.00161 ± 0.00124	ND[d]	NA[e]
K$_{p,CSF:plasma}$ = $\frac{AUC_{CSF}}{AUC_{plasma}}$	0.0085 ± 0.0021	0.0099 ± 0.0068	NS

[a]Mean ± S.D.
[b]NS, not significant; $P > 0.05$.
[c]AUC$_{0-\infty}$ (AUC$_{0-180\ min}$ by trapezoidal rule + C$_{180\ min}$/terminal phase rate constant).
[d]ND, not determined.
[e]NA, not applicable.

TABLE 2

The WSSR and AIC for control data sets vs. the calcitriol-treated data for the fitted compartment models (shown in Fig. 1)

| | | Statistic Parameters | | | |
| | | Control[a] | | Calcitriol-Treated | |
Model	Description	WSSR[b]	AIC[c]	WSSR	AIC
I	Set k_{15} = 0 for control and treatment groups; no constraints for volumes	225	−1429	160	−794
IA	Set k_{15} = 0 (same as model I); assign fitted $V_{1,plasma}$ and $V_{5,CSF}$ estimates from control data fit to the treatment group	225	−1429	158	−810
IB	Set k_{15} = 0 (same as model I); assign fitted $V_{1,plasma}$, $V_{5,CSF}$, and k_{51} estimates from control data fit to the treatment group	225	−1429	173	−454
II	Set k_{15} and k_{51} = 0 for control and treatment groups; no constraints for volumes	230	−1361	163	−628
IIA	Set k_{15} and k_{51} = 0 (same as model II); assign fitted $V_{1,plasma}$ and $V_{6,CSF}$ estimates from control data fit to the treatment group	230	−1361	170	−485
IIB	Set k_{15} and k_{51} = 0 (same as model II); assign fitted $V_{1,plasma}$, $V_{6,CSF}$, k_{56}, and k_{61} estimates from control data fit to the treatment group	230	−1361	181	−198
III	Set k_{15}, k_{16}, k_{51}, and k_{61} = 0 for control and treatment groups; no constraints for volumes	227	−1292	176	−261
IIIA	Set k_{15}, k_{16}, k_{51}, and k_{61} = 0 (same as model III); assign fitted $V_{1,plasma}$ and $V_{7,CM}$ estimates from control data fit to the treatment group	227	−1292	184	−229
IIIB	Set k_{15}, k_{16}, k_{51}, and k_{61} = 0 (same as model III); assign fitted $V_{1,plasma}$, $V_{7,CM}$, k_{56}, k_{67}, k_{78}, and k_{81} estimates from control data fit to the treatment group	227	−1292	187	−307

[a]F score for the fitted control data sets for models I, II, and III (and the A and B versions) was calculated as $\left[\frac{(SSR_j - SSR_i)}{SSR_i}\right] \times \left[\frac{df_i}{(df_j - df_i)}\right]$, in which $df_j > df_i$, and was compared with the critical F value, which was obtained from the F table with the numerator as df_j-df_i and denominator as df_i. The F score was compared with the critical F value with significance level $\alpha = 0.05$. The scores for the control and calcitriol data were not significant vs. model I (unpublished data).
[b]WSSR was provided by ADAPT5.
[c]AIC, a measurement of the goodness-of-fit, provided by ADAPT5.

treatment and not for model IA nor model IB (Table 3). For model II, the fitted values of most of the constants were unchanged, but high CVs were observed. For model III, in which there is underprediction of CSF data, there were minor changes in the CSF flow-rate constants, k_{67} and k_{78}, and k_{50}, which increased with calcitriol treatment. CL_{plasma} for model II was double that of model I for control data, and treatment increased the value from 44.5 to 55.9 ml min^{-1} kg^{-1} insignificantly (Supplemental Table 1), whereas CL_{plasma} for model III was similar to that of model I, and the value remained unchanged with calcitriol treatment (Supplemental Table 2). Overall, model I is best, but models I and II fail to explain the ratio, $k_{41}/k_{45} < 1$, which is inconsistent with known abundances of P-gp in the BBB (Qosa et al., 2014; Morris et al., 2017); only model III has the correct pattern.

Commonality of the Models. Generally speaking, there is faster equilibration between the central and peripheral compartments than with the brain compartment (k_{14}) for all of the models (see Supplemental Tables 1 and 2; Table 1). The transfer rate constant from plasma to brain (k_{14}) is slow among the distributional rate constants; k_{15} is even slower, and the fit was not altered when its value was set to zero; the efflux rate constants at the BBB (k_{41}) and ventricular barrier (k_{45}) are faster than the influx constants from plasma, k_{14} and k_{15}. All of the brain/CSF distributional rate constants (k_{14}, k_{41}, k_{45}, k_{51}, and k_{54}) are much slower than k_{12}, k_{13}, k_{21}, and k_{31}, the distributional rate constants between plasma and the peripheral compartments 1 and 2.

Modeling and Simulations. To further understand the pharmacokinetics of hAβ$_{40}$, simulations were performed based on the fitted

TABLE 3

Maximum-Likelihood Expectation Maximization population parameters for simultaneous fit of intravenous and intracerebroventricular hAβ$_{40}$ data with models I, IA, and IB (k_{15} assigned as 0) with fitting by ADAPT5

| | Control Rats: Fit 1 | Calcitriol-Treated Rats: Fit 2 | | |
| | Model I | Model I | Model IA $V_{1,plasma}$ and $V_{5,CSF}$ Same as Model I | Model IB V_1, V_5, and k_{51} Same as Model I |
Population-fitted parameters[a]	i.v. (n = 16[b]) and i.c.v. (n = 4)	i.v. (n = 7) and i.c.v. (n = 5)	i.v. (n = 7) and i.c.v. (n = 5)	i.v. (n = 7) & i.c.v. (n = 5)
k_{10} (min^{-1})	0.186 ± 0.0901	0.206 ± 0.0335	0.176 ± 0.0823	0.231 ± 0.0506
k_{12} (min^{-1})	0.164 ± 0.0416	0.140 ± 0.0575	0.195 ± 0.0796	0.141 ± 0.112
k_{13} (min^{-1})	0.0524 ± 0.0255	0.0426 ± 0.0207	0.0479 ± 0.0133	0.0468 ± 0.00727*
k_{14} (min^{-1})	0.0000523 ± 0.0000172	0.0000690 ± 0.0000229*	0.0000605 ± 0.0000232	0.0000868 ± 0.0000411*
k_{21} (min^{-1})	0.245 ± 0.0942	0.271 ± 0.132	0.367 ± 0.216*	0.279 ± 0.0920
k_{31} (min^{-1})	0.0430 ± 0.0120	0.0492 ± 0.0196	0.0603 ± 0.0322	0.0415 ± 0.00437
k_{40} (min^{-1})	0.0131 ± 0.00619	0.0139 ± 0.00311	0.0148 ± 0.00389	0.0124 ± 0.00278
k_{41} (min^{-1})	0.000105 ± 0.0000287	0.000188 ± 0.0000302*	0.000181 ± 0.0000600*	0.000131 ± 0.0000318*
k_{45} (min^{-1})	0.00274 ± 0.00154	0.00938 ± 0.00446*	0.00439 ± 0.00167*	0.00754 ± 0.00513*
k_{50} (min^{-1})	0.0110 ± 0.00117	0.0114 ± 0.00126	0.0137 ± 0.00168*	0.0117 ± 0.00132*
k_{51} (min^{-1})	0.00146 ± 0.000787	0.00791 ± 0.00548*	0.0120 ± 0.00841*	0.00146 ± 0.000787
k_{54} (min^{-1})	0.0722 ± 0.0154	0.0754 ± 0.0472	0.180 ± 0.124*	0.435 ± 0.187*
$V_{1,plasma}$ (ml)	33.1 ± 26.7	42.4 ± 15.2	33.1 (fixed)	33.1 (fixed)
$V_{5,CSF}$ (ml)	0.417 ± 0.203	2.20 ± 1.84*	0.417 (fixed)	0.417 (fixed)
$CL_{plasma} = k_{10} \cdot V_{1,plasma}$ (ml·min^{-1}·kg^{-1})	21.8	25.8*	17.2	22.6

[a]Mean ± S.D. (CV%) of parameter estimate.
[b]Pooled intravenously injected mice (with or without corn oil injections, n = 16).
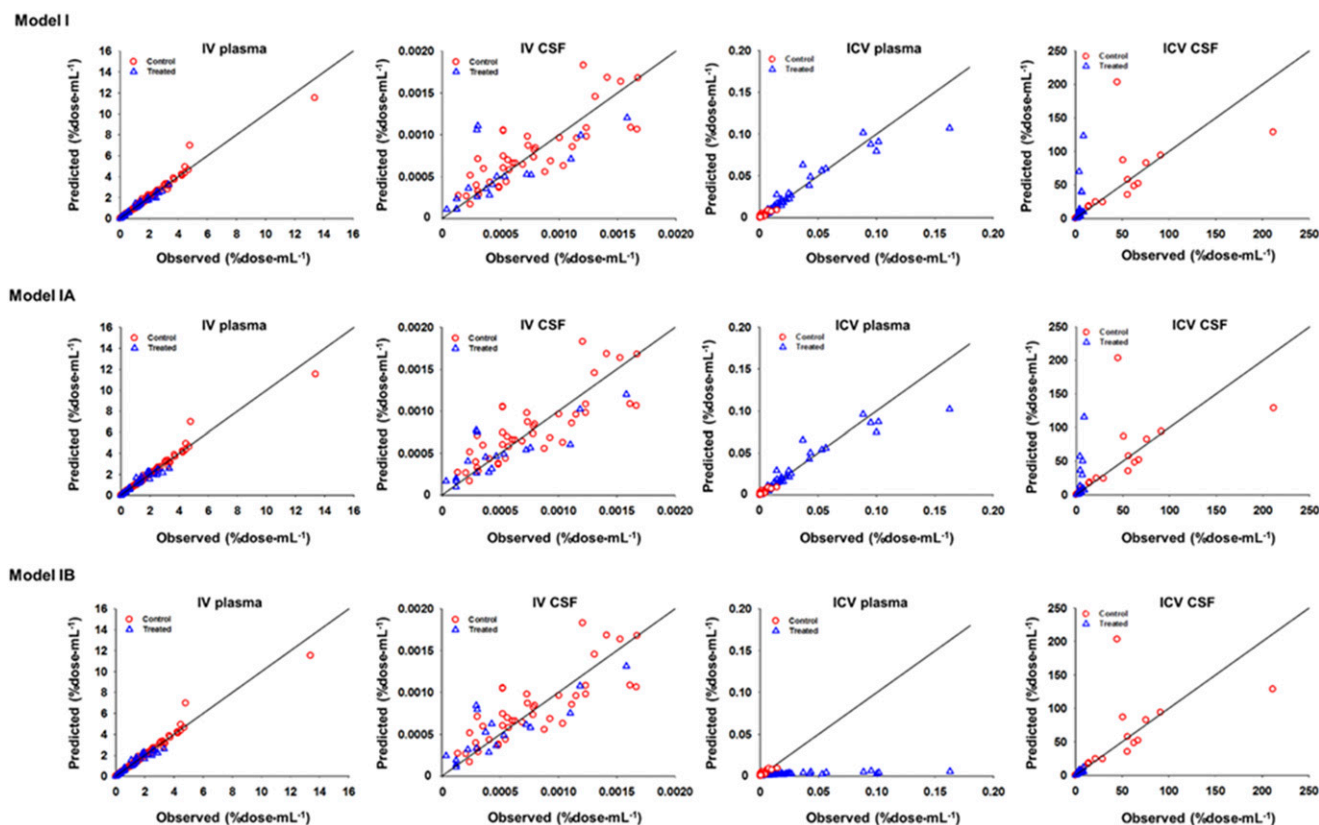*$P < 0.05$, Wilcoxon rank sum test (nonparametric test, conducted in R), from individual fits (unpublished data).

Fig. 4. Prediction plots for model I (upper panel), model IA (middle panel, setting and V$_{1,plasma}$ and V$_{5,CSF}$ constant as those for model I), and model IB (bottom panel, setting and V$_{1,plasma}$, V$_{5,CSF}$, and k$_{51}$ constant as those for model I) after intravenous (IV) and intracerebroventricular (ICV) injections; serial samples obtained from the same rat were denoted with the same symbol. The black line represents the line of identity.

parameters of the best model, model I. The amount of hAβ$_{40}$ in brain (expressed as %dose) was normalized to the brain volume (1.8 g) (Davies and Morris, 1993). Plasma concentrations were shown to decay more rapidly with a shorter plasma t$_{1/2}$ after intravenous versus intracerebroventricular injection, but then plasma levels tapered off, and levels became parallel to those for the brain and CSF (Fig. 6). This is due to the rapid distribution of hAβ$_{40}$ (k$_{12}$ and k$_{13}$) to the peripheral compartments and very slow permeation (k$_{14}$ and k$_{15}$ ~0) into the brain and CSF. The return of hAβ$_{40}$ from brain and CSF (k$_{41}$ and k$_{51}$)

to the circulation were also slower than k$_{21}$ and k$_{31}$ (Supplemental Tables 1 and 2; Table 1), and with time, the terminal t$_{1/2}$ of the plasma, brain, and CSF for hAβ$_{40}$ all became similar (Fig. 6). The slow distribution rate constants k$_{41}$ and k$_{51}$ relative to the faster k$_{21}$ and k$_{31}$ rate constants rate limit the distribution of hAβ$_{40}$ from brain/CSF back to plasma, resulting in an apparently faster plasma t$_{1/2}$ after intravenous administration. For intracerebroventricular administration, CSF and brain levels are closer to the injection site, and the CSF t$_{1/2}$ paralleled that in plasma.
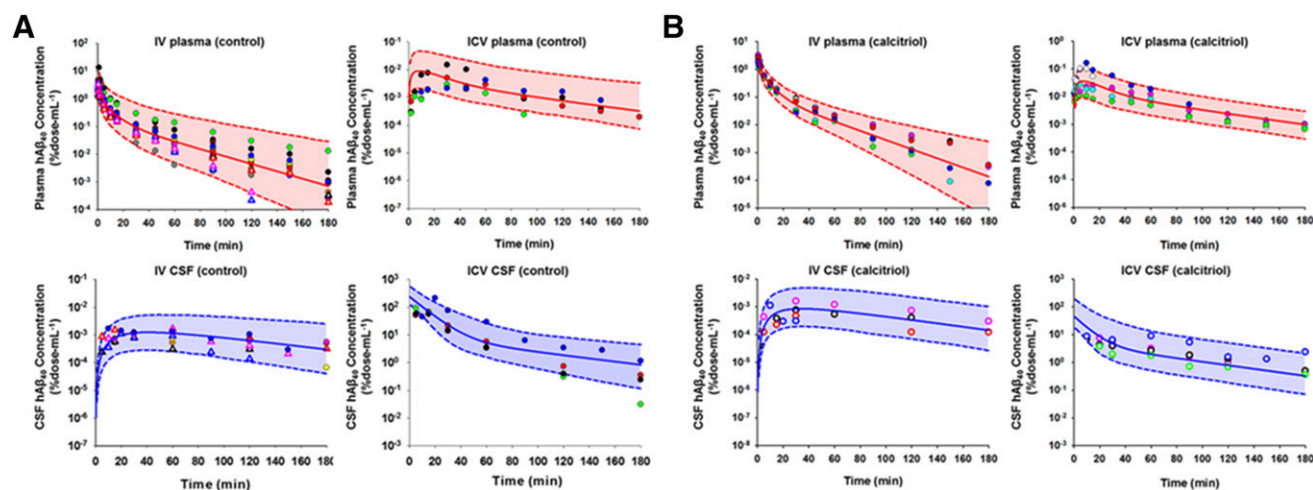

Fig. 5. Fits of observed vs. predicted plasma and CSF concentrations in control and calcitriol-treated rats after hAβ$_{40}$ intravenous (IV) and intracerebroventricular (ICV) administration (data of Fig. 4) to model I. The red and blue lines represent the lines of best fit for plasma and CSF, respectively, and the shaded regions denote the 5% and 95% confidence interval. Serial samples obtained from the same rat were denoted with the same symbol.
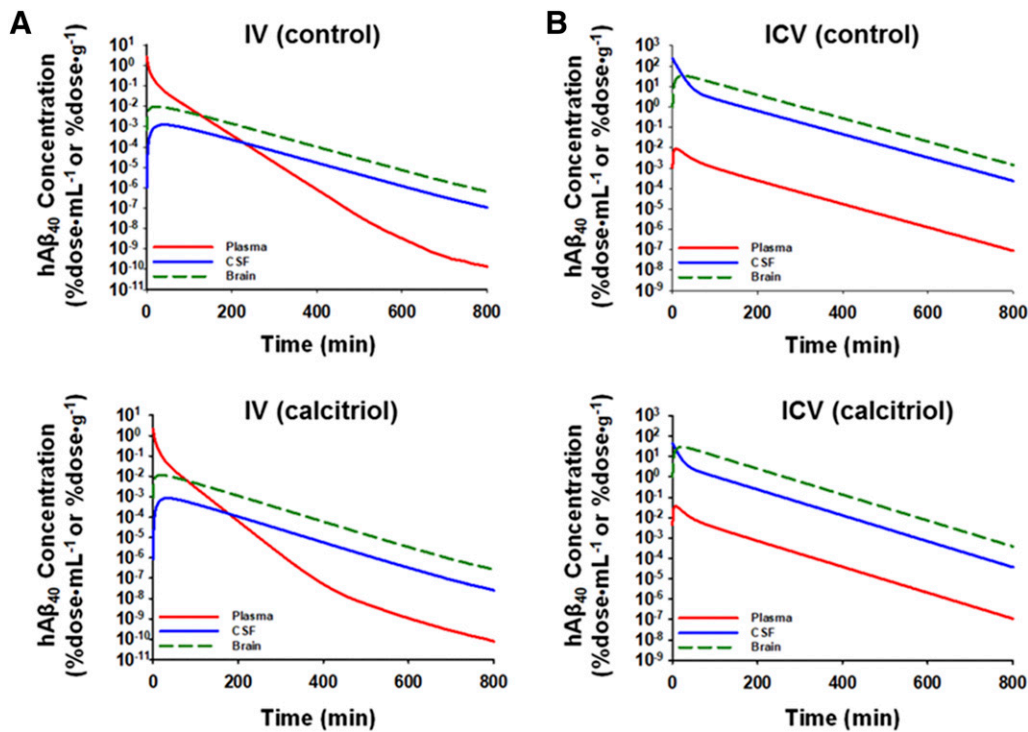
Fig. 6. Simulations based on fitted parameters for model I (Table 3) >800 minutes for plasma, brain, and CSF concentrations after hAβ$_{40}$ was given as single intravenous (IV) and intracerebroventricular (ICV) injections, with and without calcitriol treatment.

The simulated AUC$_\infty$s for model I further revealed other dispositional patterns of the administration route and induction by calcitriol (Table 4). The route of the injection results in higher AUC$_\infty$ for the injected site, for example, plasma exposure (AUC$_{\infty,\text{plasma,IV}}$) after intravenous administration is higher than after intracerebroventricular administration, and the pattern persists with absence or presence of calcitriol treatment (Fig. 6; Tables 3 and 4). Similarly, CSF exposure (AUC$_{\infty,\text{CSF,ICV}}$) is much higher after intracerebroventricular administration than intravenous administration, and the pattern also persists with or without calcitriol treatment. There is little change in AUC$_{\infty,\text{brain}}$ after intravenous or intracerebroventricular administration or calcitriol treatment, suggesting that this parameter is relatively insensitive to calcitriol-mediated changes in brain hAβ$_{40}$ disposition (Table 3). The AUC$_{\infty,\text{plasma,IV}}$ is much higher than AUC$_{\infty,\text{brain,IV}}$ and AUC$_{\infty,\text{CSF,IV}}$ after intravenous administration because of the slow distribution of hAβ$_{40}$ into brain and CSF (Table 4). The AUC$_{\infty,\text{CSF,ICV}}$ is similar to AUC$_{\infty,\text{brain,ICV}}$, and these greatly exceed AUC$_{\infty,\text{plasna,ICV}}$ after intracerebroventricular administration, reflecting

slow efflux of k$_{41}$ and k$_{51}$ at the BBB and BCSFB/BAB (Table 3). Overall, calcitriol treatment resulted in a substantial reduction of AUC$_{\infty,\text{plasma,IV}}$ and AUC$_{\infty,\text{CSF,IV}}$ after intravenous administration according to model I, and there is decreased AUC$_{\infty,\text{CSF,ICV}}$ but increased AUC$_{\infty,\text{plasma,ICV}}$ after intracerebroventricular administration because of the increases in k$_{41}$ (BBB), k$_{45}$, and k$_{51}$ (Table 4).

Western Immunoblot for Efflux and Degradation Proteins

P-gp, Neprilysin, Lrp1, and Mrp1 Relative Protein Expressions. Western immunoblotting was conducted to determine the relative protein changes in brain P-gp and Mrp1, neprilysin, and Lrp1 for the efflux transporters and degradation enzyme(s) in the crude-brain non-nuclear membrane fraction. Samples from the corn oil–treated controls (hAβ$_{40}$ intravenous) were compared with the calcitriol-treated rats (intravenous and intracerebroventricular hAβ$_{40}$). Calcitriol treatment resulted in a significant increase (~2-fold) in P-gp protein expression in the rat brain, an observation similar to that observed in mouse (Chow

TABLE 4

Simulated AUC$_{0-\infty}$ for plasma, brain, and CSF to yield partition coefficients (K$_p$) based on fitted parameters with model I (Table 3) for calcitriol-treated and control rats

|	Control: Fit 1 (Untreated)	Treatment: Fit 2 (Calcitriol in Corn Oil i.p.)	Ratio (Treated/Control)			
	i.v.	i.c.v.	i.v.	i.c.v.	i.v.	i.c.v.
AUC$_{\infty,\text{plasma}}$ (%dose·min·ml^{-1})	16.2	0.435	11.4	1.52		3.49
					0.70	
AUC$_{\infty,\text{brain}}$ (%dose·min·ml^{-1})	1.14	3482	1.17	2812		0.81
					1.03	
AUC$_{\infty,\text{CSF}}$ (%dose·min·ml^{-1})	0.159	3319	0.095	709		0.214
					0.597	
K$_{\text{p,brain:plasma}} = \frac{\text{AUC}_{\infty,\text{brain}}}{\text{AUC}_{\infty,\text{plasma}}}$	0.0700	8007	0.102	1847		0.231
					1.45	
K$_{\text{p,CSF:plasma}} = \frac{\text{AUC}_{\infty,\text{CSF}}}{\text{AUC}_{\infty,\text{plasma}}}$	0.00983	7633	0.00827	466		0.051
					0.842	
$\frac{\text{AUC}_{\infty,\text{CSF}}}{\text{AUC}_{\infty,\text{brain}}}$	0.140	0.953	0.0811	0.252		0.264
					0.58	
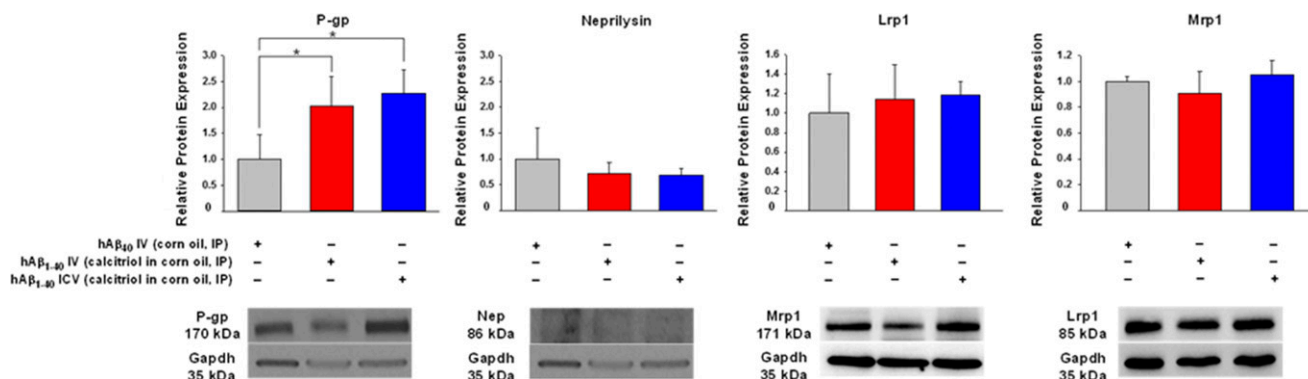
Fig. 7. Relative brain P-gp, neprilysin, Lrp1 and Mrp1 protein expressions in corn oil-treated control and calcitriol-treated rats were determined by Western Immunoblotting as described under Methods; * P < 0.05 denotes significance. The background-corrected signals of P-gp (170 kDa) and neprilysin (85.5 kDa) in the same sample were separated on the same gel, and normalized to the intensity of the house-keeping gene, Gapdh (36 kDa). Separate gels were individually used for the determination of Lrp1 (85 kDa) and Mrp1 (172 kDa).

et al., 2011) and rat (Durk et al., 2015), and agreed with the predictions of models I and IA (1.79- and 1.72-fold increase in k_{41}). However, neprilysin, Lrp1, and Mrp1 relative protein expression levels were unchanged with calcitriol treatment (Fig. 7). Levels of Bcrp protein expression were also not altered, as we found previously (Durk et al., 2012). The lack of change neprilyin protein agreed with the lack of change in the degradation rate constant (k_{40}) in the brain.

Discussion

Being assured that our strategy of using multiple calibration curves circumvented the sample matrix interference problem in the ELISA assay (Fig. 2), we proceeded to define the pharmacokinetics of hAβ_{40}. After intravenous injection, a low biliary clearance (0.00161 ± 0.00124 ml·min^{-1}·kg^{-1}) and even lower (undetectable) renal clearance were noted for hAβ_{40}. The apparent plasma $t_{1/2}$ and intravenous plasma clearance were 24.5 minutes and 18–22 ml·min^{-1}·kg^{-1}, respectively (Table 1), and these observations are compatible with those in mice ($t_{1/2}$ = 25.5 minutes) (Shibata et al., 2000) and rats (Saito et al., 1995), in which the $t_{1/2}$ was 27 minutes, and V_{ss} was 273 ± 59 ml·kg^{-1}. Kandimalla et al. (2005, 2006) reported faster I^{125}-Aβ_{40} half-lives of 9.2 ± 2.3 and 11.2 ± 5.1 minutes after intravenous administration and longer half-lives of 30 and 50 minutes in a later study (Kandimalla et al., 2007). CL$_{plasma}$ was 10.1 ± 1.2 ml·min^{-1}·kg^{-1} (Kandimalla et al., 2005, 2006) after intravenous administration of the radioactively labeled peptide and 5.48 ± 0.38 and 4.58 ± 0.57 ml·min^{-1}·kg^{-1}, respectively, in 2- and 25-month-old mice (Nishida et al., 2009). These smaller clearance values were likely due to radiolabeled metabolites present that contributed to a higher area under the curve. Our data suggest that intravenously injected hAβ_{40} crosses from plasma into the brain and CSF slowly and that hAβ_{40}, when injected into the rat CSF after intracerebroventricular injection, is detected in the systemic circulation, as found by others (Ghersi-Egea et al., 1996b; Spies et al., 2012; Tarasoff-Conway et al., 2015), suggesting that hAβ_{40} is able to traverse from the CSF to plasma via the BCSFB, CSF flow, or arachnoid barrier (Fig. 3). A notable observation is the faster $t_{1/2}$ for plasma but a slightly longer $t_{1/2}$ for CSF (76 minutes) within 180 minutes in our intravenous studies (Fig. 3). The lower concentrations of hAβ_{40} in CSF after intravenous dosing agree with other studies, showing that Aβ permeability from plasma into brain (via BBB) or CSF (via k_{15}, BCSFB) is poor (Saito et al., 1995; Poduslo et al., 1999; Kandimalla et al., 2005). Interestingly, reports on intracerebral administration of ^{125}I-Aβ_{40} concluded that the major clearance pathways are via the BBB or degradation, whereas efflux across BCSFB via bulk transport is

diminutive (Shiiki et al., 2004; Yamada et al., 2008; Qosa et al., 2014), and that ^{125}I-Aβ_{40} administered into CSF via intracerebroventricular diffuses into brain tissue poorly and is cleared from CSF to blood (same for^{125}I-BDNF and ^{14}C-sucrose) (Yan et al., 1994; Ghersi-Egea et al., 1996a,b).

We modeled the intravenous and intracerebroventricular data based on models I, II, and III and variations thereof. In model I (Fig. 1A), the brain compartment is associated with intercompartmental rates constants k_{14} and k_{41} at the BBB and k_{15} and k_{51} at the BCSFB/choroid plexus, although the return clearance of $V_{5,CSF}$ k_{51}, denotes return from the ventricular CSF (BCSFB), CSF bulk flow, and P-gp efflux at the arachnoid villi (BAB) to the central compartment. Modification of model I with more CSF compartments provided more physiologic relevance but did not improve the fits (Fig. 1). The F scores showed that fixing the volumes (version "A") or the CSF return clearance terms ($V_{5,CSF}k_{51}$, $V_{6,CSF}k_{61}$, or $V_{8,CSF}k_{81}$) (version "B") or assignment of physiologic volumes (Davies and Morris, 1993; Yamamoto et al., 2018) did not significantly alter the F score (Table 2). This is because the models, being catenary in nature with interconnections between brain and CSF with plasma, and the brain with CSF rendered more uncertainty/ambiguity. Therefore, we used the prediction plots (Fig. 4; Supplemental Figs. 1 and 2) and established models I and IA as the best models. Model I predicts that P-gp efflux at the BBB (k_{41}) and BAB (k_{51}) is increased by calcitriol treatment. The trend for the 2-fold increase in P-gp protein expression in brain (Fig. 7) is in agreement with model I predictions (Table 3). The influx of hAβ_{40} by P-gp into the CSF at the choroid plexus (k_{15}) is unimportant since inclusion or deletion of k_{15} did not alter the fit. However, the model also predicts that calcitriol treatment results in a 3.4-fold increase in k_{45}, the rate constant for transfer of hAβ_{40} from brain into CSF via the leaky ependymal cells in the ventricles. Model II, although with high CV in the fits, is also acceptable. Model III fits are poor.

Although P-gp protein expression is predominantly expressed apically at the BBB, there is controversy over the localization of P-gp at the BCSFB. Rao et al. (1999) demonstrated the presence of P-gp apically in primary culture of the choroid plexus epithelial cells from 1-week-old neonatal rat's lateral and fourth ventricles, but others failed to detect P-gp apically at the choroid plexus among rats of different ages (Gazzin et al., 2008; Roberts et al., 2008; Pascale et al., 2011; Yasuda et al., 2013). According to brain anatomy, the choroid plexus is only a portion of the BCSFB. The arachnoid epithelium (arachnoid mater) lining the subarachnoid space where the CSF fills (above the pia mater) constitutes another barrier (Yasuda et al., 2013) and the cranial and spinal arachnoid villi constitute the predominant site of CSF clearance

into the venous outflow system (Sakka et al., 2011). Especially when the efflux from BCSFB is slow, the sum of this efflux and CSF flow and efflux of the BAB constitute the return clearance from CSF to the blood compartment, ($k_{51} \cdot V_{5,CSF}$), which was increased 5.4-fold according to model I (Table 3). It should be noted that other clearance processes also exist, such as degradation processes by microglia and other enzymes (insulin degradation enzyme, angiotensin, and/or endothelin-converting enzyme) (Saido and Leissring, 2012).

With model I being the best and simplest model, the disparity in the $t_{1/2}$ was explained with simulations based on the slow distribution constants k_{14}, k_{15}, k_{41}, and k_{51} between plasma and brain/CSF in comparison with the faster constants (k_{12}, k_{13}, k_{21}, and k_{31}) between plasma and peripheral compartments (Supplemental Tables 1 and 2; Table 3). The difference in $t_{1/2}$ between plasma and CSF within the 180-minute observation period after intravenous injection disappeared at around 600 minutes, revealing the slower terminal γ phase of about 50–60 minutes in plasma that paralleled the $t_{1/2}$ in CSF and brain after intravenous dosing (Fig. 6). Because of the slow transfer rate constant to brain (k_{14}) or CSF ($k_{15} = 0$) as rate-limiting steps after intravenous dosing and k_{41} and k_{51} after intracerebroventricular dosing, we noted that the K_p values are different because of differences in AUC$_\infty$s in the plasma and CSF (based on simulations) and their dependence on the route of administration (Table 4). We also showed that the specific site of injection of hAβ_{40} may lead to preferential routes of clearance by the brain, as shown by others (Shiiki et al., 2004; Yamada et al., 2008; Qosa et al., 2014), whether hAβ_{40} is effluxed across BBB or undergoes brain enzymatic degradation. Substrates administered into brain tissue by intracerebral injections are preferentially cleared via the BBB, whereas substrates given by intracerebroventricular injections into the CSF are preferentially cleared via the BCSFB/BAB and CSF bulk flow. hAβ_{40} distribution into the CSF is not a measure of BBB permeability but is a measure of transport across the choroid plexus (k_{15}) as well as the arachnoid barrier (k_{51}) and k_{45}, efflux at the ventricular barrier. The CSF is a not a homogeneous space in brain parenchyma, and a substrate injected into CSF will distribute in a pattern stepwise along the ventricles to perfuse brain tissue at the arachnoid villi and ependymal surface of brain or spinal cord and then return to blood.

To conclude, it was shown that matrix interference in the ELISA method was circumvented by appropriate calibration curves prepared in sample matrix. After verification that corn oil did not affect hAβ_{40} kinetics or concentration-time profile, we established that model I best fit the data from intravenous and intracerebroventricular injections in both untreated and calcitriol-treated rats. Calcitriol treatment altered hAβ_{40} disposition via the induction of P-gp, increasing efflux at the BBB (increase in k_{41}) and maybe the BAB (increase in k_{51}). Although calcitriol treatment induced P-gp protein expression by 2-fold, other clearance mechanisms may exist, particularly at the arachnoid villi barrier. The model predicts a slow equilibration between plasma and CSF due to slow permeation of hAβ_{40} to the brain and CSF, but when data were simulated over a long period of time, the $t_{1/2}$ and levels of hAβ_{40} in plasma, CSF, and brain all decayed in unison. Under this circumstance, the plasma hAβ_{40} profile would better reflect that in the brain. Hence, those using plasma hAβ_{40} as a biomarker by itself or as a ratio with hAβ_{42} to reflect brain concentrations or AD progression must proceed with caution.

Authorship Contributions

Participated in research design: Peng, de Lannoy, Pang.

Conducted experiments: Peng, Noh, Pan, Saldivia, Serson, Toscan.

Performed data analysis: Peng, Noh, Pang.

Wrote or contributed to the writing of the manuscript: Peng, de Lannoy, Pang.

References

Abramowski D, Wiederhold KH, Furrer U, Jaton AL, Neuenschwander A, Runser MJ, Danner S, Reichwald J, Ammaturo D, Staab D, et al. (2008) Dynamics of Abeta turnover and deposition in different beta-amyloid precursor protein transgenic mouse models following gamma-secretase inhibition. *J Pharmacol Exp Ther* **327**:411–424.

Alemi M, Gaiteiro C, Ribeiro CA, Santos LM, Gomes JR, Oliveira SM, Couraud PO, Weksler B, Romero I, Saraiva MJ, et al. (2016) Transthyretin participates in beta-amyloid transport from the brain to the liver--involvement of the low-density lipoprotein receptor-related protein 1? *Sci Rep* **6**:20164.

Bateman RJ, Munsell LY, Morris JC, Swarm R, Yarasheski KE, and Holtzman DM (2006) Human amyloid-beta synthesis and clearance rates as measured in cerebrospinal fluid *in vivo*. *Nat Med* **12**:856–861.

Bates KA, Verdile G, Li QX, Ames D, Hudson P, Masters CL, and Martins RN (2009) Clearance mechanisms of Alzheimer's amyloid-beta peptide: implications for therapeutic design and diagnostic tests. *Mol Psychiatry* **14**:469–486.

Bell RD, Sagare AP, Friedman AE, Bedi GS, Holtzman DM, Deane R, and Zlokovic BV (2007) Transport pathways for clearance of human Alzheimer's amyloid beta-peptide and apolipoproteins E and J in the mouse central nervous system. *J Cereb Blood Flow Metab* **27**:909–918.

Biere AL, Ostaszewski B, Stimson ER, Hyman BT, Maggio JE, and Selkoe DJ (1996) Amyloid beta-peptide is transported on lipoproteins and albumin in human plasma. *J Biol Chem* **271**: 32916–32922.

Boxenbaum HG, Riegelman S, and Elashoff RM (1974) Statistical estimations in pharmacokinetics. *J Pharmacokinet Biopharm* **2**:123–148.

Chow EC, Durk MR, Cummins CL, and Pang KS (2011) 1alpha,25-dihydroxyvitamin D3 upregulates P-glycoprotein via the vitamin D receptor and not farnesoid X receptor in both fxr(-/-) and fxr(+/+) mice and increased renal and brain efflux of digoxin in mice in vivo. *J Pharmacol Exp Ther* **337**:846–859.

Cirrito JR, May PC, O'Dell MA, Taylor JW, Parsadanian M, Cramer JW, Audia JE, Nissen JS, Bales KR, Paul SM, et al. (2003) *In vivo* assessment of brain interstitial fluid with microdialysis reveals plaque-associated changes in amyloid-beta metabolism and half-life. *J Neurosci* **23**: 8844–8853.

Davies B and Morris T (1993) Physiological parameters in laboratory animals and humans. *Pharm Res* **10**:1093–1095.

Deane R, Bell RD, Sagare A, and Zlokovic BV (2009) Clearance of amyloid-beta peptide across the blood-brain barrier: implication for therapies in Alzheimer's disease. *CNS Neurol Disord Drug Targets* **8**:16–30.

de Lange ECM, van den Brink W, Yamamoto Y, de Witte WEA, and Wong YC (2017) Novel CNS drug discovery and development approach: model-based integration to predict neuropharmacokinetics and pharmacodynamics. *Expert Opin Drug Discov* **12**:1207–1218.

Durk MR, Chan GN, Campos CR, Peart JC, Chow EC, Lee E, Cannon RE, Bendayan R, Miller DS, and Pang KS (2012) 1α,25-Dihydroxyvitamin D₃-liganded vitamin D receptor increases expression and transport activity of P-glycoprotein in isolated rat brain capillaries and human and rat brain microvessel endothelial cells. *J Neurochem* **123**:944–953.

Durk MR, Fan J, Sun N, Yang Y, Pang H, Pang KS, and de Lannoy IA (2015) Vitamin D receptor activation induces P-glycoprotein and increases brain efflux of quinidine: an intracerebral microdialysis study in conscious rats. *Pharm Res* **32**:1128–1140.

Durk MR, Han K, Chow EC, Ahrens R, Henderson JT, Fraser PE, and Pang KS (2014) 1α,25-Dihydroxyvitamin D3 reduces cerebral amyloid-β accumulation and improves cognition in mouse models of Alzheimer's disease. *J Neurosci* **34**:7091–7101.

Gazzin S, Strazielle N, Schmitt C, Fevre-Montange M, Ostrow JD, Tiribelli C, and Ghersi-Egea JF (2008) Differential expression of the multidrug resistance-related proteins ABCb1 and ABCc1 between blood-brain interfaces. *J Comp Neurol* **510**:497–507.

Ghersi-Egea JF, Finnegan W, Chen JL, and Fenstermacher JD (1996a) Rapid distribution of intraventricularly administered sucrose into cerebrospinal fluid cisterns via subarachnoid velae in rat. *Neuroscience* **75**:1271–1288.

Ghersi-Egea JF, Gorevic PD, Ghiso J, Frangione B, Patlak CS, and Fenstermacher JD (1996b) Fate of cerebrospinal fluid-borne amyloid beta-peptide: rapid clearance into blood and appreciable accumulation by cerebral arteries. *J Neurochem* **67**:880–883.

Ghiso J, Shayo M, Calero M, Ng D, Tomidokoro Y, Gandy S, Rostagno A, and Frangione B (2004) Systemic catabolism of Alzheimer's Abeta40 and Abeta42. *J Biol Chem* **279**: 45897–45908.

Haass C, Koo EH, Mellon A, Hung AY, and Selkoe DJ (1992) Targeting of cell-surface beta-amyloid precursor protein to lysosomes: alternative processing into amyloid-bearing fragments. *Nature* **357**:500–503.

Hardy JA and Higgins GA (1992) Alzheimer's disease: the amyloid cascade hypothesis. *Science* **256**:184–185.

Hartmann T, Bieger SC, Brühl B, Tienari PJ, Ida N, Allsop D, Roberts GW, Masters CL, Dotti CG, Unsicker K, et al. (1997) Distinct sites of intracellular production for Alzheimer's disease A beta40/42 amyloid peptides. *Nat Med* **3**:1016–1020.

Iwata N, Higuchi M, and Saido TC (2005) Metabolism of amyloid-beta peptide and Alzheimer's disease. *Pharmacol Ther* **108**:129–148.

Iwata N, Tsubuki S, Takaki Y, Watanabe K, Sekiguchi M, Hosoki E, Kawashima-Morishima M, Lee HJ, Hama E, Sekine-Aizawa Y, et al. (2000) Identification of the major Abeta1-42-degrading catabolic pathway in brain parenchyma: suppression leads to biochemical and pathological deposition. *Nat Med* **6**:143–150.

Jan A, Hartley DM, and Lashuel HA (2010) Preparation and characterization of toxic Abeta aggregates for structural and functional studies in Alzheimer's disease research. *Nat Protoc* **5**: 1186–1209.

Kandimalla KK, Curran GL, Holasek SS, Gilles EJ, Wengenack TM, and Poduslo JF (2005) Pharmacokinetic analysis of the blood-brain barrier transport of ^{125}I-amyloid beta protein 40 in wild-type and Alzheimer's disease transgenic mice (APP,PS1) and its implications for amyloid plaque formation. *J Pharmacol Exp Ther* **313**:1370–1378.

Kandimalla KK, Curran GL, Holasek SS, Gilles EJ, Wengenack TM, Ramirez-Alvarado M, and Poduslo JF (2006) Physiological and biophysical factors that influence Alzheimer's disease amyloid plaque targeting of native and putrescine modified human amyloid beta40. *J Pharmacol Exp Ther* **318**:17–25.

Kandimalla KK, Wengenack TM, Curran GL, Gilles EJ, and Poduslo JF (2007) Pharmacokinetics and amyloid plaque targeting ability of a novel peptide-based magnetic resonance contrast agent in wild-type and Alzheimer's disease transgenic mice. *J Pharmacol Exp Ther* **322**:541–549.

Kuo YM, Emmerling MR, Lampert HC, Hempelman SR, Kokjohn TA, Woods AS, Cotter RJ, and Roher AE (1999) High levels of circulating Abeta42 are sequestered by plasma proteins in Alzheimer's disease. *Biochem Biophys Res Commun* **257**:787–791.

Lam FC, Liu R, Lu P, Shapiro AB, Renoir JM, Sharom FJ, and Reiner PB (2001) beta-Amyloid efflux mediated by p-glycoprotein. *J Neurochem* **76**:1121–1128.

Lanz TA and Schachter JB (2006) Demonstration of a common artifact in immunosorbent assays of brain extracts: development of a solid-phase extraction protocol to enable measurement of amyloid-beta from wild-type rodent brain. *J Neurosci Methods* **157**:71–81.

Lowry OH, Rosebrough NJ, Farr AL, and Randall RJ (1951) Protein measurement with the Folin phenol reagent. *J Biol Chem* **193**:265–275.

Maarouf CL, Walker JE, Sue LI, Dugger BN, Beach TG, and Serrano GE (2018) Impaired hepatic amyloid-beta degradation in Alzheimer's disease. *PLoS One* **13**:e0203659.

Marques MA, Kulstad JJ, Savard CE, Green PS, Lee SP, Craft S, Watson GS, and Cook DG (2009) Peripheral amyloid-beta levels regulate amyloid-beta clearance from the central nervous system. *J Alzheimers Dis* **16**:325–329.

Mawuenyega KG, Sigurdson W, Ovod V, Munsell L, Kasten T, Morris JC, Yarasheski KE, and Bateman RJ (2010) Decreased clearance of CNS beta-amyloid in Alzheimer's disease. *Science* **330**:1774 Available from: 10.1126/science.1197623.

Morris ME, Rodriguez-Cruz V, and Felmlee MA (2017) SLC and ABC transporters: expression, localization, and species differences at the blood-brain and the blood-cerebrospinal fluid barriers. *AAPS J* **19**:1317–1331.

Nishida Y, Ito S, Ohtsuki S, Yamamoto N, Takahashi T, Iwata N, Jishage K, Yamada H, Sasaguri H, Yokota S, et al. (2009) Depletion of vitamin E increases amyloid beta accumulation by decreasing its clearances from brain and blood in a mouse model of Alzheimer disease. *J Biol Chem* **284**:33400–33408.

Pardridge WM (2016) CSF, blood-brain barrier, and brain drug delivery. *Expert Opin Drug Deliv* **13**:963–975.

Pascale CL, Miller MC, Chiu C, Boylan M, Caralopoulos IN, Gonzalez L, Johanson CE, and Silverberg GD (2011) Amyloid-beta transporter expression at the blood-CSF barrier is age-dependent. *Fluids Barriers CNS* **8**:21.

Poduslo JF, Curran GL, Sanyal B, and Selkoe DJ (1999) Receptor-mediated transport of human amyloid beta-protein 1-40 and 1-42 at the blood-brain barrier. *Neurobiol Dis* **6**:190–199.

Qosa H, Abuasal BS, Romero IA, Weksler B, Couraud PO, Keller JN, and Kaddoumi A (2014) Differences in amyloid-β clearance across mouse and human blood-brain barrier models: kinetic analysis and mechanistic modeling. *Neuropharmacology* **79**:668–678.

Rao VV, Dahlheimer JL, Bardgett ME, Snyder AZ, Finch RA, Sartorelli AC, and Piwnica-Worms D (1999) Choroid plexus epithelial expression of MDR1 P glycoprotein and multidrug resistance-associated protein contribute to the blood-cerebrospinal-fluid drug-permeability barrier. *Proc Natl Acad Sci USA* **96**:3900–3905.

Roberts LM, Black DS, Raman C, Woodford K, Zhou M, Haggerty JE, Yan AT, Cwirla SE, and Grindstaff KK (2008) Subcellular localization of transporters along the rat blood-brain barrier and blood-cerebral-spinal fluid barrier by in vivo biotinylation. *Neuroscience* **155**:423–438.

Roychaudhuri R, Zheng X, Lomakin A, Maiti P, Condron MM, Benedek GB, Bitan G, Bowers MT, and Teplow DB (2015) Role of species-specific primary structure differences in Aβ42 assembly and neurotoxicity. *ACS Chem Neurosci* **6**:1941–1955.

Saido T and Leissring MA (2012) Proteolytic degradation of amyloid β-protein. *Cold Spring Harb Perspect Med* **2**:a006379.

Saito Y, Buciak J, Yang J, and Pardridge WM (1995) Vector-mediated delivery of 125I-labeled beta-amyloid peptide A beta 1-40 through the blood-brain barrier and binding to Alzheimer disease amyloid of the A beta 1-40/vector complex. *Proc Natl Acad Sci USA* **92**:10227–10231.

Sakka L, Coll G, and Chazal J (2011) Anatomy and physiology of cerebrospinal fluid. *Eur Ann Otorhinolaryngol Head Neck Dis* **128**:309–316.

Seppälä TT, Herukka SK, Hänninen T, Tervo S, Hallikainen M, Soininen H, and Pirttilä T (2010) Plasma Abeta42 and Abeta40 as markers of cognitive change in follow-up: a prospective, longitudinal, population-based cohort study. *J Neurol Neurosurg Psychiatry* **81**:1123–1127.

Shibata M, Yamada S, Kumar SR, Calero M, Bading J, Frangione B, Holtzman DM, Miller CA, Strickland DK, Ghiso J, et al. (2000) Clearance of Alzheimer's amyloid-ss(1-40) peptide from brain by LDL receptor-related protein-1 at the blood-brain barrier. *J Clin Invest* **106**:1489–1499.

Shiiki T, Ohtsuki S, Kurihara A, Naganuma H, Nishimura K, Tachikawa M, Hosoya K, and Terasaki T (2004) Brain insulin impairs amyloid-beta(1-40) clearance from the brain. *J Neurosci* **24**:9632–9637.

Spies PE, Verbeek MM, van Groen T, and Claassen JA (2012) Reviewing reasons for the decreased CSF Abeta42 concentration in Alzheimer disease. *Front Biosci* **17**:2024–2034.

Stine WB Jr., Dahlgren KN, Krafft GA, and LaDu MJ (2003) *In vitro* characterization of conditions for amyloid-beta peptide oligomerization and fibrillogenesis. *J Biol Chem* **278**:11612–11622.

Tamaki C, Ohtsuki S, Iwatsubo T, Hashimoto T, Yamada K, Yabuki C, and Terasaki T (2006) Major involvement of low-density lipoprotein receptor-related protein 1 in the clearance of plasma free amyloid beta-peptide by the liver. *Pharm Res* **23**:1407–1416.

Tang C, Kuo Y, Pudvah NT, Ellis JD, Michener MS, Egbertson M, Graham SL, Cook JJ, Hochman JH, and Prueksaritanont T (2009) Effect of P-glycoprotein-mediated efflux on cerebrospinal fluid concentrations in rhesus monkeys. *Biochem Pharmacol* **78**:642–647.

Tarasoff-Conway JM, Carare RO, Osorio RS, Glodzik L, Butler T, Fieremans E, Axel L, Rusinek H, Nicholson C, Zlokovic BV, et al. (2015) Clearance systems in the brain-implications for Alzheimer disease. *Nat Rev Neurol* **11**:457–470.

Takasawa K, Terasaki T, Suzuki H, Ooie T, and Sugiyama Y (1997) Distributed model analysis of 3′-azido-3′-deoxythymidine and 2′,3′-dideoxyinosine distribution in brain tissue and cerebrospinal fluid. *J Pharmacol Exp Ther* **282**:1509–1517.

Teplow DB (2006) Preparation of amyloid beta-protein for structural and functional studies. *Methods Enzymol* **413**:20–33.

Vergallo A, Mégret L, Lista S, Cavedo E, Zetterberg H, Blennow K, Vanmechelen E, De Vos A, Habert MO, Potier MC, et al.; INSIGHT-preAD study group; ; Alzheimer Precision Medicine Initiative (APMI) (2019) Plasma amyloid β 40/42 ratio predicts cerebral amyloidosis in cognitively normal individuals at risk for Alzheimer's disease. *Alzheimers Dement* **15**:764–775.

Weidemann A, Paliga K, Dürrwang U, Reinhard FB, Schuckert O, Evin G, and Masters CL (1999) Proteolytic processing of the Alzheimer's disease amyloid precursor protein within its cytoplasmic domain by caspase-like proteases. *J Biol Chem* **274**:5823–5829.

Westerhout J, Ploeger B, Smeets J, Danhof M, and de Lange EC (2012) Physiologically based pharmacokinetic modeling to investigate regional brain distribution kinetics in rats. *AAPS J* **14**:543–553.

Yamada K, Hashimoto T, Yabuki C, Nagae Y, Tachikawa M, Strickland DK, Liu Q, Bu G, Basak JM, Holtzman DM, et al. (2008) The low density lipoprotein receptor-related protein 1 mediates uptake of amyloid beta peptides in an *in vitro* model of the blood-brain barrier cells. *J Biol Chem* **283**:34554–34562.

Yamamoto Y, Välitalo PA, Wong YC, Huntjens DR, Proost JH, Vermeulen A, Krauwinkel W, Beukers MW, Kokki H, Kokki M, et al. (2018) Prediction of human CNS pharmacokinetics using a physiologically-based pharmacokinetic modeling approach. *Eur J Pharm Sci* **112**:168–179.

Yan Q, Matheson C, Sun J, Radeke MJ, Feinstein SC, and Miller JA (1994) Distribution of intracerebral ventricularly administered neurotrophins in rat brain and its correlation with trk receptor expression. *Exp Neurol* **127**:23–36.

Yasojima K, McGeer EG, and McGeer PL (2001) Relationship between beta amyloid peptide generating molecules and neprilysin in Alzheimer disease and normal brain. *Brain Res* **919**:115–121.

Yasuda K, Cline C, Vogel P, Onciu M, Fatima S, Sorrentino BP, Thirumaran RK, Ekins S, Urade Y, Fujimori K, et al. (2013) Drug transporters on arachnoid barrier cells contribute to the blood-cerebrospinal fluid barrier. *Drug Metab Dispos* **41**:923–931.

Zlokovic BV, Yamada S, Holtzman D, Ghiso J, and Frangione B (2000) Clearance of amyloid beta-peptide from brain: transport or metabolism? *Nat Med* **6**:718–719.

Address correspondence to: Dr. K. Sandy Pang, Department of Pharmaceutical Sciences, Leslie Dan Faculty of Pharmacy, University of Toronto, 144 College St., Toronto, Ontario, Canada M5S 3M2. E-mail: ks.pang@utoronto.ca

Supplemental Tables and Figures

Human β-Amyloid 40 (hAβ40) Kinetics after Intravenous (IV) and Intracerebroventricular (ICV) Injections and Calcitriol Treatment in

Rats *in vivo*

H. Benson Peng, Keumhan Noh, Sophie R. Pan, Victor Saldivia, Sylvia Serson, Anja Toscan, Inés A.M. de Lannoy[†], and K. Sandy

Pang[†]

[†]co-senior authors

Department of Pharmaceutical Sciences (H.B.P., K.N., K.S.P.), Leslie Dan Faculty of Pharmacy,

University of Toronto

and

InterVivo Solutions Inc. (V.S., S.R.P., S.S., A.T., I.A.L.), Brampton, Ontario, Canada

Supplemental Table 1. MLEM population parameters for simultaneous fit of IV and ICV hAβ$_{40}$ data with Models II, IIA and IIB by ADAPT5[®]

Population Fitted Parameters[a]	Control Rats – Fit 1	Calcitriol Treated Rats – Fit 2		
	Model II	Model II	Model IIA $V_{1,plasma}$ and $V_{6,CSF}$ as Model II	Model IIB $V_{1,plasma}$, $V_{6,CSF}$, k_{56}, & k_{61} as Model II
	IV (n = 16[b]) & ICV (n = 4)	IV (n = 7) & ICV (n = 5)	IV (n = 7) & ICV (n = 5)	IV (n = 7) & ICV (n = 5)
k_{10} (min^{-1})	0.181 ± 0.0936	0.509 ± 0.557	0.317 ± 0.334	0.314 ± 0.317
k_{12} (min^{-1})	0.135 ± 0.0468	0.124 ± 0.0358	0.0656 ± 0.0232*	0.0891 ± 0.0257*
k_{13} (min^{-1})	0.0458 ± 0.0217	0.0461 ± 0.00800	0.0344 ± 0.00271*	0.0363 ± 0.00539*
k_{21} (min^{-1})	0.223 ± 0.0895	0.249 ± 0.0841	0.247 ± 0.0578	0.248 ± 0.0254
k_{14} (min^{-1})	0.000280 ± 0.000128	0.000301 ± 0.0000423	0.000240 ± 0.0000477*	0.000334 ± 0.000120
k_{15} (min^{-1})	0	0	0	0
k_{31} (min^{-1})	0.0477 ± 0.0210	0.0433 ± 0.0109	0.0457 ± 0.00618	0.0526 ± 0.00751
k_{40} (min^{-1})	0.324 ± 0.142	0.338 ± 0.0526	0.356 ± 0.0533	0.350 ± 0.103*
k_{41} (min^{-1})	0.000929 ± 0.0000986	0.000920 ± 0.000105	0.000910 ± 0.0000891	0.000931 ± 0.0000930
k_{45} (min^{-1})	0.00276 ± 0.00143	0.00285 ± 0.000394	0.00237 ± 0.000461*	0.00331 ± 0.00117
k_{50} (min^{-1})	0.00316 ± 0.000418	0. 0.00344 ± 0.000630	0.00315 ± 0.000369	0.00454 ± 0.00130*
k_{51} (min^{-1})	0	0	0	0
k_{54} (min^{-1})	0.00122 ± 0.000128	0.00124 ± 0.000143	0.00132 ± 0.000138*	0.00137 ± 0.000168*
k_{56} (min^{-1})	0.0689 ± 0.0321	0.360 ± 0.518	0.784 ± 1.12*	0.0689 (fixed)
k_{61} (min^{-1})	0.0222 ± 0.00715	0.0234 ± 0.00413	0.0218 ± 0.00686	0.0222 (fixed)
$V_{1,plasma}$ (mL)	69.4 ± 150	37.2 ± 7.58	69.4 (fixed)	69.4 (fixed)
$V_{6,CSF}$ (mL)	0.574 ± 0.187	1.73 ± 2.46	0.574 (fixed)	0.574 (fixed)
CL_{plasma} = $k_{10} \cdot V_{1,plasma}$ (mL·min^{-1}·kg^{-1})	44.5	55.9	64.9	21.8

[a]Mean ±S.D. (CV%) of parameter estimate
[b]Pooled IV injected mice (with or without corn oil injections, n=16)
*P < 0.05, Wilcoxon rank sum test (nonparametric test, conducted in R); from individual fits (data not shown)

Supplemental Table 2. MLEM population parameters for simultaneous fit of IV and ICV hAβ_{40} data with Model III, IIIA and IIIB by ADAPT5®

Population Fitted Parameters[a]	Control Rats – Fit 1	Calcitriol Treated Rats – Fit 2		
	Model III	Model III	Model IIIA $V_{1,plasma}$ & $V_{7,CM}$ same as Model III	Model IIIB $V_{1,plasma}, V_{7,CM}, k_{56}, k_{67}, k_{78},$ & k_{81} same as Model III
	IV (n = 16[b]) & ICV (n = 4)	IV (n = 7) & ICV (n = 5)	IV (n = 7) & ICV (n = 5)	IV (n = 7) & ICV (n = 5)
k_{10} (min^{-1})	0.266 ± 0.115	0.227 ± 0.0274	0.173 ± 0.00888*	0.171 ± 0.00846*
k_{12} (min^{-1})	0.135 ± 0.0273	0.146 ± 0.0204	0.108 ± 0.0108*	0.112 ± 0.0119*
k_{13} (min^{-1})	0.0470 ± 0.0229	0.0463 ± 0.00604	0.0394 ± 0.00372*	0.0407 ± 0.00400*
k_{14} (min^{-1})	0.00301 ± 0.000498	0.00391 ± 0.000415*	0.00369 ± 0.000373*	0.00323 ± 0.000423*
k_{15} (min^{-1})	0	0	0	0
k_{16} (min^{-1})	0	0	0	0
k_{21} (min^{-1})	0.236 ± 0.0878	0.218 ± 0.0400	0.247 ± 0.0236	0.241 ± 0.0233
k_{31} (min^{-1})	0.0440 ± 0.0136	0.0510 ± 0.00508	0.0547 ± 0.00542*	0.0547 ± 0.00543*
k_{40} (min^{-1})	0.335 ± 0.124	0.304 ± 0.0315	0.323 ± 0.0321	0.361 ± 0.0459
k_{41} (min^{-1})	0.0128 ± 0.00220	0.0123 ± 0.00130	0.0121 ± 0.00128	0.0119 ± 0.00120*
k_{45} (min^{-1})	0.00279 ± 0.000440	0.00358 ± 0.000381*	0.00340 ± 0.000349*	0.00296 ± 0.000383
k_{50} (min^{-1})	0.381 ± 0.0798	0.465 ± 0.0596*	0.561 ± 0.0963*	2.64 ± 0.747*
k_{51} (min^{-1})	0	0	0	0
k_{54} (min^{-1})	0.0126 ± 0.00210	0.0121 ± 0.00127	0.0121 ± 0.00128	0.0121 ± 0.00121
k_{56} (min^{-1})	0.0425 ± 0.00662	0.0305 ± 0.00497*	0.0233 ± 0.00480*	0.0425
k_{61} (min^{-1})	0	0	0	0
k_{67} (min^{-1})	0.0595 ± 0.0567	0.0186 ± 0.00242*	0.0181 ± 0.00221*	0.0595
k_{78} (min^{-1})	0.0422 ± 0.0103	0.0741 ± 0.0116*	0.0810 ± 0.0138*	0.0422
k_{81} (min^{-1})	0.0103 ± 0.00901	0.00743 ± 0.000748	0.00735 ± 0.000744	0.0103
$V_{1,plasma}$ (mL)	28.4 ± 16.2	35.0 ± 9.47	28.4 (fixed)	28.4 (fixed)
$V_{7,CM}$ (mL)	0.117 ± 0.0399	0.190 ± 0.0314*	0.117 (fixed)	0.117 (fixed)
$CL_{plasma} = k_{10} \cdot V_{1,plasma}$ (mL·min^{-1} kg^{-1})	26.8	23.4	14.5*	14.3*

[a]Mean ±S.D. (CV%) of parameter estimate
[b]Pooled IV injected mice (with or without corn oil injections, n=16)
*$P < 0.05$, Wilcoxon rank sum test (nonparametric test, conducted in R); from individual fits (data not shown)

Supplemental Figure 1. Prediction plots for Model II (upper panel), Model IIA (middle panel, setting and $V_{1,plasma}$ and $V_{6,CSF}$ constant as those for Model II) and Model IIB (bottom panel, setting and $V_{1,plasma}$ $V_{6,CSF}$ and k_{61} constant as those for Model II) after IV and ICV injections.
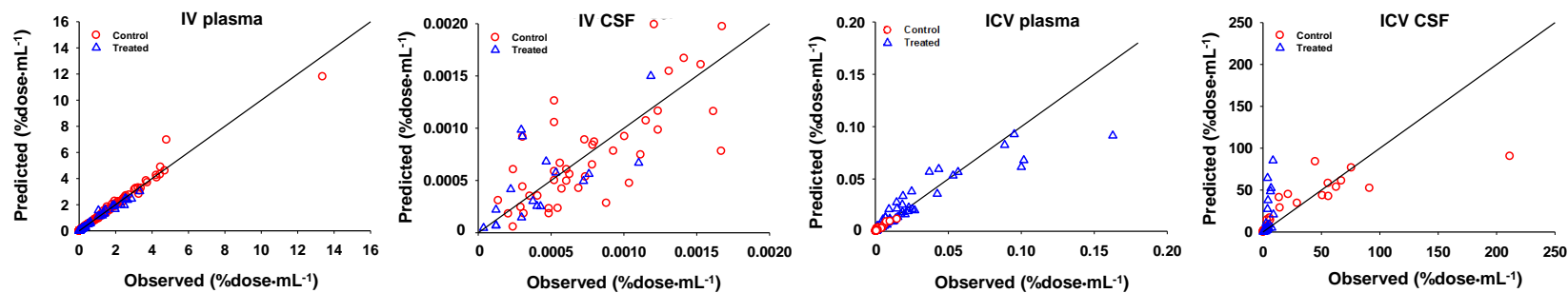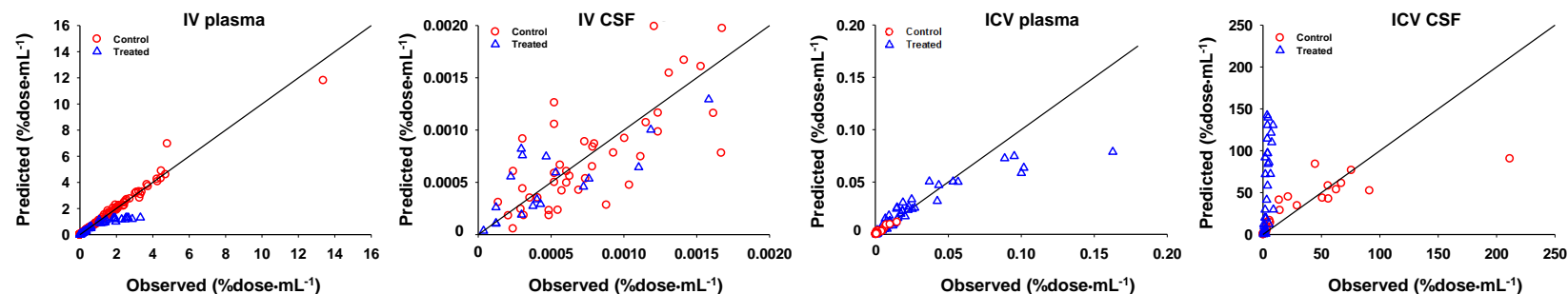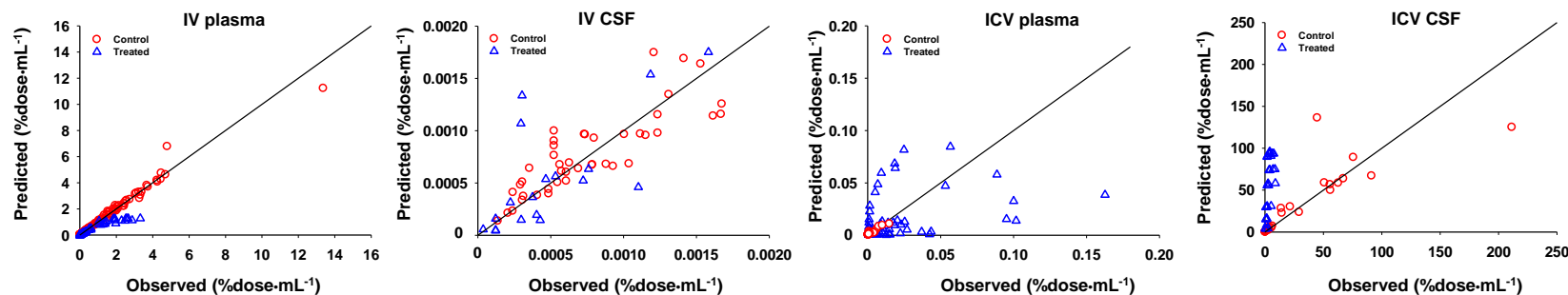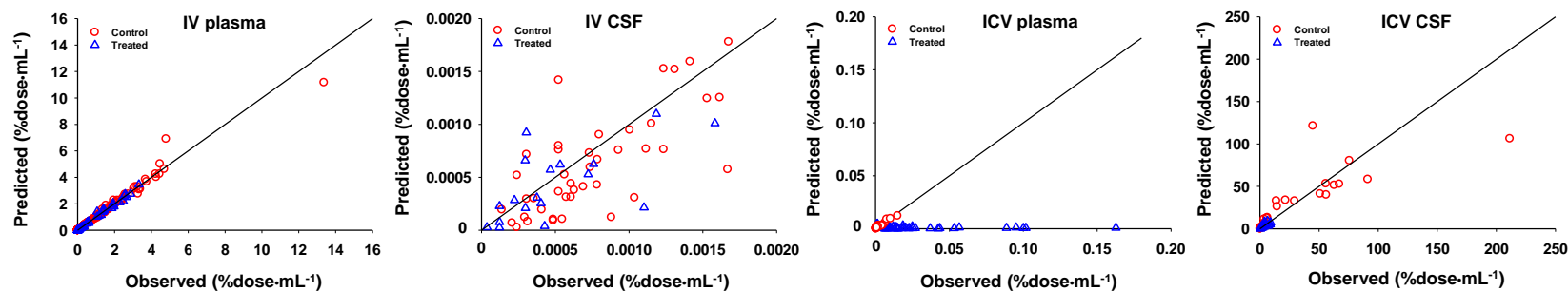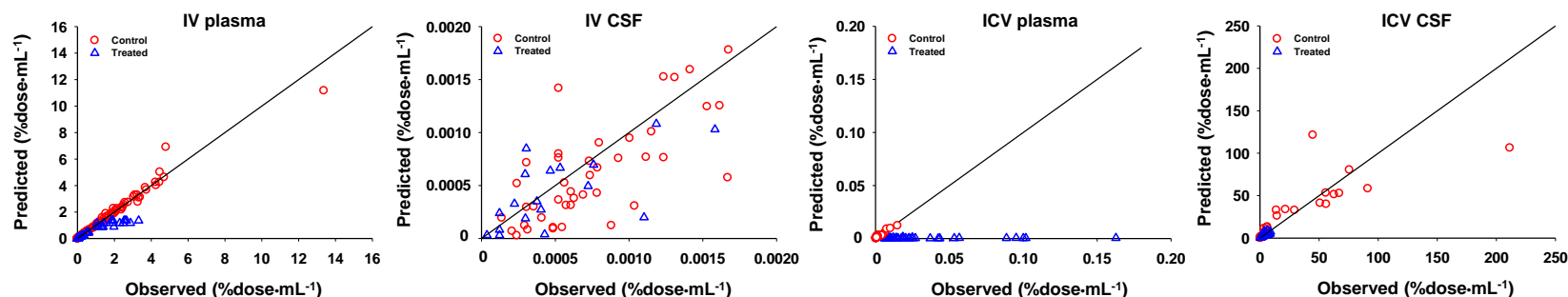
Supplemental Figure 2. Prediction plots for Model III (upper panel), Model IIIA (middle panel, setting and $V_{1,plasma}$ and $V_{8,CSF}$ constant as those for Model III) and Model IIIB (bottom panel, setting and $V_{1,plasma}$ $V_{8,CSF}$ and k_{81} constant as those for Model III) after IV and ICV injections.